

# Solitonic ground states in (color-) superconductivity

Dominik Nickel<sup>1</sup> and Michael Buballa<sup>2</sup>

<sup>1</sup>*Center for Theoretical Physics, MIT, Cambridge, MA 02139, USA*

<sup>2</sup>*Institut für Kernphysik, Technische Universität Darmstadt, Germany*

(Dated: September 21, 2020)

We present a general framework for analyzing inhomogeneous (color-) superconducting phases in mean-field approximation without restriction to the Ginzburg-Landau approach. As a first application, we calculate real gap functions with general one-dimensional periodic structures for a  $3 + 1$ -dimensional toy model having two fermion species. The resulting solutions are energetically favored against homogeneous superconducting (BCS) and normal conducting phases in a window for the chemical potential difference  $\delta\mu$  which is about twice as wide as for the most simple plane-wave ansatz (“Fulde-Ferrell phase”). At the lower end of this window, we observe the formation of a soliton lattice and a continuous phase transition to the BCS phase. At the higher end of the window the gap functions are sinusoidal, and the transition to the normal conducting phase is of first order. We also discuss the quasiparticle excitation spectrum in the inhomogeneous phase. Finally, we compare the gap functions with the known analytical solutions of the  $1 + 1$ -dimensional theory.

## I. INTRODUCTION

Inhomogeneous ground states due to imbalanced Fermi surfaces have been discussed in various contexts. Theoretical investigations started off by considering a clean paramagnetic superconductor exposed to an external magnetic field. For such a system Fulde and Ferrell analyzed the ground state with the order parameter, i.e., the gap function, forming a plane wave [1]. Larkin and Ovchinnikov extended their work by considering more general inhomogeneous ground states, but relying on the Ginzburg-Landau expansion [2].

In recent years these ideas have attracted new interest from two fields. One of them are systems of ultracold atoms [3], where new fascinating techniques open unprecedented possibilities to study the pairing of imbalanced Fermi systems in a trap. Here, unlike in solids where the electron interaction is often difficult to understand in detail, imbalanced systems can be prepared in a rather straight forward and controlled way.

In this paper, we will mainly aim at color superconductivity in deconfined quark matter. Here the problem of imbalanced Fermi surfaces is almost unavoidable. It is expected that color superconducting phases are present in the QCD phase diagram at sufficiently high densities and low temperatures (see Refs. [4–10] for corresponding reviews). In nature, the most promising places to find these conditions are the centers of neutron stars. Here the system must be in beta equilibrium and, at least globally, electrically and color neutral. This would be fulfilled if there were equally many up-, down-, and strange quarks. However, at densities which can be reached in neutron stars, strange quarks are expected to be considerably suppressed by their mass. In turn, this forces the density of down quarks to be larger than the density of up quarks in order to achieve electric neutrality. Since, on the other hand, the most attractive channels

involve quarks of unequal flavors, we are naturally led to the problem of pairing in an imbalanced Fermi system [11–21].

Let us briefly recall what the problem actually is. In BCS theory, pairing occurs among fermions with opposite momenta, forming Cooper pairs with zero total momentum. If both fermions are at their respective Fermi surface, the pair can be created at no free-energy cost and the pairing is always favored as soon as there is an attractive interaction. This is, however, no longer the case if the Fermi momenta of the fermions to be paired are unequal. BCS pairing then requires that the Fermi spheres first have to be equalized. In the case of quark matter this could be realized, e.g., in a weak process which replaces some of the down quarks by strange quarks. Of course, this will only be favorable if the free energy which is needed for this process is overcompensated by the pairing energy. This sets a limit for this mechanism in terms of the Fermi momentum difference in the unpaired system and the BCS gap [22].

Therefore the question arises how the system reacts if the imbalance does no longer allow for BCS-like pairing. Sticking to homogeneous phases, some authors have suggested so-called gapless or breached pairing phases [23–26], where equal Fermi surfaces are created by lifting some of the fermions to higher momentum states. At these “new” Fermi surfaces the fermions can again form Cooper pairs with zero total momentum. It was found, however, that this pairing mechanism suffers from instabilities [27, 28]. In atomic systems this will most likely lead to a phase separation into a BCS-like phase with equal densities and an unpaired phase with unequal densities. In principle, something similar could happen in quark matter as well [12, 29, 30]. However, because of long-range Coulomb forces, the different phase domains cannot grow arbitrarily large, and it is therefore unclear whether a mixed phase can exist at all.

Instead, it seems reasonable that the matter becomes

inhomogeneous already on a microscopic scale by the formation of “crystalline condensates” (see Ref. [31] for a dedicated review). The basic idea is to form Cooper pairs with non-zero total momentum. This has the obvious advantage that the fermions in the pair no longer have to have opposite momenta, and therefore each of them can stay on its respective Fermi surface. In the context of color superconductors, this possibility has been investigated first in Ref. [32]. The authors restricted themselves to a two-flavor model with a plane-wave ansatz for the gap function, like in the original work by Fulde and Ferrell [1]. Indeed, as was shown in Ref. [33], one of the instabilities which occur in gapless two-flavor color superconductors could be related to an instability against the formation of a Fulde-Ferrell (FF) -like condensate.

On the other hand, since in the FF ansatz the total momentum of the pair is restricted to a non-zero but constant value  $2\vec{q}$ , this pairing pattern is strongly disfavored by phase space in most cases. Several authors have therefore extended the ansatz to multiple plane waves, studying both, two- and three-flavor systems [34–37]. As expected, the resulting solutions were found to be strongly favored against the FF phase. However, these analyses were restricted to a Ginzburg-Landau approximation. This turned out to be especially problematic in the two-flavor case, where the Ginzburg-Landau functional for the energetically favored solution was not bounded from below [34]. Moreover, the crystal structures considered so far have been restricted to superpositions of a finite number of plane waves whose wave vectors all have the same length, whereas one should also allow for the superposition of different wave lengths.

The aim of this paper is to overcome the restriction to the Ginzburg-Landau approximation and to approach the mean-field problem explicitly. The thermodynamic potential is then always bounded from below and a proper treatment leads to new insights which could not be obtained in the previous investigations. As a first step we will focus on two-flavor pairing allowing an arbitrary real gap functions with general one-dimensional periodic structure.

For inhomogeneous ground states the mean-field problem is already non-trivial and requires to solve the Bogoliubov-de Gennes equations [38]. Only for  $1 + 1$ -dimensional systems there is a good understanding of the mean-field ground state and the thermodynamic properties of the system [39–45]. This is, however, lacking for higher dimensional systems and attempts have been made to simplify these equations, e.g., by integrating out short-range fluctuations [46, 47]. We will not pursue such a direction here, but instead present a numerical approach to solve the Bogoliubov-de Gennes equations in a convenient basis. The presentation and derivation is elementary so that no prior knowledge of inhomogeneous phases is required. It turns out that at least for relativistic systems the regularization of the theory has to be addressed carefully in order to avoid undesired artifacts.

The paper is organized as follows: In section II we

introduce the model we aim to investigate in a certain approximation and derive an expression for the thermodynamic potential in an inhomogeneous phase together with the corresponding gap equation. Because of its importance for inhomogeneous phases in  $3 + 1$ -dimensions, we also discuss a suitable regularization scheme. In section III we then present numerical results for inhomogeneous phases with one-dimensional inhomogeneity in  $3 + 1$ -dimensions. As a prelude we discuss the homogeneous (color-)superconducting and the Fulde-Ferrell phase first, before confronting them with results for a general pairing pattern. For the latter we continue by exploring the quasi-particle spectrum and a comparison to analytical results obtained in  $1 + 1$ -dimensions. Finally we summarize our results in section IV and give an outlook for possible further investigations.

## II. FORMALISM

In this section we develop the general framework for the description of inhomogeneous color-superconducting phases.

### A. Model Lagrangian

We consider an NJL-type Lagrangian for massless quarks  $q$  with three flavor and three color degrees of freedom,

$$\mathcal{L} = \bar{q}(i\cancel{\partial} + \not{\mu})q + \mathcal{L}_{int}. \quad (1)$$

We have introduced the notation  $\not{\mu} = \mu\gamma^0$ , where  $\mu$  is the chemical potential. To be precise,  $\mu$  is a diagonal matrix in color-flavor space, allowing for different chemical potentials for different colors or flavors.

The interaction term is given by

$$\mathcal{L}_{int} = H \sum_{A,A'=2,5,7} (\bar{q} i\gamma_5 \tau_A \lambda_{A'} q_C)(\bar{q}_C i\gamma_5 \tau_A \lambda_{A'} q). \quad (2)$$

Here  $H$  is a dimensionful coupling constant and  $q_C(x) = C\bar{q}^T(x)$ , where  $C = i\gamma^2\gamma^0$  is the matrix of charge conjugation.  $\tau_A$  and  $\lambda_{A'}$  denote the antisymmetric Gell-Mann matrices acting in flavor space and color space, respectively. Thus,  $\mathcal{L}_{int}$  corresponds to a quark-quark interaction in the scalar flavor-antitriplet color antitriplet channel.

The above Lagrangian should be viewed as a typical example which allows for the most important pairing patterns in color superconductivity, like the two-flavor superconducting (2SC) phase and the color-flavor locked (CFL) phase. However, the formalism we are going to develop in this section is by no means restricted to this model. In particular we may add mass terms, and the inclusion of other interaction channels is straight forward.

Applying standard bosonization techniques, the interaction term, Eq. (2), can equivalently be rewritten as

$$\mathcal{L}_{int} = \frac{1}{2} \sum_{A,A'} \left\{ (\bar{q} \gamma_5 \tau_A \lambda_{A'} q_C) \varphi_{AA'} - \varphi_{AA'}^\dagger (\bar{q}_C \gamma_5 \tau_A \lambda_{A'} q) - \frac{1}{2H} \varphi_{AA'}^\dagger \varphi_{AA'} \right\}, \quad (3)$$

with the auxiliary complex boson fields  $\varphi_{AA'}(x)$ , which, by the equations of motion,

$$\begin{aligned} \varphi_{AA'}(x) &= -2H \bar{q}_C(x) \gamma_5 \tau_A \lambda_{A'} q(x), \\ \varphi_{AA'}^\dagger(x) &= 2H \bar{q}(x) \gamma_5 \tau_A \lambda_{A'} q_C(x), \end{aligned} \quad (4)$$

can be identified with scalar diquarks.

In mean field approximation we replace these quantum fields by their expectation values

$$\begin{aligned} \langle \varphi_{AA'}(x) \rangle &= \Delta_A(x) \delta_{AA'}, \\ \langle \varphi_{AA'}^\dagger(x) \rangle &= \Delta_A^*(x) \delta_{AA'}, \end{aligned} \quad (5)$$

where the ‘‘gap function’’  $\Delta_A(x)$  is now a classical field. Here we assume that the condensation takes place only in the diagonal flavor-color components of the gap matrix,  $A = A'$ , as in the standard ansatz for the CFL or the 2SC phase. Note, however, that we retain the full space-time dependence of the field.

Introducing Nambu-Gor'kov bispinors,

$$\Psi(x) = \frac{1}{\sqrt{2}} \begin{pmatrix} q(x) \\ q_C(x) \end{pmatrix}, \quad \bar{\Psi}(x) = \frac{1}{\sqrt{2}} (\bar{q}(x), \bar{q}_C(x)), \quad (6)$$

we obtain the effective mean-field Lagrangian

$$\mathcal{L}_{MF}(x) = \bar{\Psi}(x) S^{-1}(x) \Psi(x) - \frac{1}{4H} \sum_A |\Delta_A(x)|^2, \quad (7)$$

with the inverse dressed quark propagator

$$S^{-1}(x) = \begin{pmatrix} i\cancel{\partial} + \cancel{\mu} & \hat{\Delta}(x) \gamma_5 \\ -\hat{\Delta}^*(x) \gamma_5 & i\cancel{\partial} - \cancel{\mu} \end{pmatrix}. \quad (8)$$

Here we used the more compact notation

$$\hat{\Delta}(x) = \sum_A \Delta_A(x) \tau_A \lambda_A, \quad (9)$$

i.e.,  $\hat{\Delta}(x)$  is a matrix in color and flavor space.

## B. Thermodynamic potential

We now consider a static crystalline structure with a unit cell spanned by three linearly independent vectors  $\vec{a}_1$ ,  $\vec{a}_2$ , and  $\vec{a}_3$ . This means, the gap matrix  $\hat{\Delta}(x)$  is time independent and periodic in space,

$$\hat{\Delta}(x) \equiv \hat{\Delta}(\vec{x}) = \hat{\Delta}(\vec{x} + \vec{a}_i), \quad i = 1, 2, 3. \quad (10)$$

Hence,  $\hat{\Delta}$  can be decomposed into a discrete set of Fourier components,

$$\hat{\Delta}(x) = \sum_{q_k} \hat{\Delta}_{q_k} e^{-iq_k \cdot x}, \quad (11)$$

where the allowed momenta are given by the conditions

$$q_k = \begin{pmatrix} 0 \\ \vec{q}_k \end{pmatrix}, \quad \vec{q}_k \cdot \vec{a}_i = 2\pi N_{ki}, \quad (12)$$

for  $N_{ki} \in \mathbb{Z}$ . These momenta form a reciprocal lattice (*R.L.*) in momentum space.

For the bispinors  $\Psi$  and  $\bar{\Psi}$  we consider a finite quantization volume  $V$  with periodic boundary conditions. Working at finite temperature  $T$  and employing Matsubara formalism the (imaginary) time variable is restricted to a finite interval as well,  $0 \leq \tau = it \leq 1/T$ . Hence, the allowed energies and three-momenta both are discrete and we have the Fourier decompositions

$$\begin{aligned} \Psi(x) &= \frac{1}{\sqrt{V}} \sum_{p_n} \Psi_{p_n} e^{-ip_n \cdot x}, \\ \bar{\Psi}(x) &= \frac{1}{\sqrt{V}} \sum_{p_n} \bar{\Psi}_{p_n} e^{ip_n \cdot x}. \end{aligned} \quad (13)$$

Here we have explicitly taken out a normalization factor  $1/\sqrt{V}$  to have dimensionless Fourier components  $\Psi_{p_n}$  and  $\bar{\Psi}_{p_n}$ .

For a consistent description of the crystal, the quantization volume should contain an integer number of unit cells. Without loss of generality we therefore assume that  $V$  is spanned by the vectors  $N\vec{a}_i$ , where  $N$  is a positive integer. Then the allowed momenta are given by

$$p_n = \begin{pmatrix} i\omega_{p_n} \\ \vec{p}_n \end{pmatrix}, \quad \vec{p}_n \cdot \vec{a}_i = 2\pi \frac{N_{ni}}{N}, \quad (14)$$

with  $\omega_{p_n}$  being fermionic Matsubara frequencies and  $N_{ni} \in \mathbb{Z}$ . Comparing this with Eq. (12), we see that the three-momenta form a mesh which, in each direction, is  $N$  times finer than the reciprocal lattice of the crystal. Later we will take the infinite volume limit,  $N \rightarrow \infty$ , where the set of allowed three-momenta becomes continuous.

The thermodynamic potential per volume is given by

$$\Omega(T, \mu) = -\frac{T}{V} \ln \mathcal{Z}(T, \mu), \quad (15)$$

where

$$\mathcal{Z}(T, \mu) = \int \mathcal{D}\Psi \mathcal{D}\bar{\Psi} e^{\mathcal{S}} \quad (16)$$

is the grand canonical partition function with the Euclidean action

$$\mathcal{S} = \int_0^{1/T} d\tau \int_V d^3x \mathcal{L}(x^0 = -i\tau, \vec{x}). \quad (17)$$

Inserting the Fourier decompositions, Eqs. (11) and (13), into Eq. (7) and turning out the integrals, we obtain in mean-field approximation

$$\mathcal{S}_{MF} = \frac{1}{T} \sum_{p_m, p_n} \bar{\Psi}_{p_m} S_{p_m, p_n}^{-1} \Psi_{p_n} - \frac{1}{4H} \frac{V}{T} \sum_A \sum_{q_k} |\Delta_{A, q_k}|^2, \quad (18)$$

where

$$S_{p_m, p_n}^{-1} = \begin{pmatrix} (\not{p}_n + \not{\mu}) \delta_{p_m, p_n} & \sum_{q_k} \hat{\Delta}_{q_k} \gamma_5 \delta_{q_k, p_m - p_n} \\ -\sum_{q_k} \hat{\Delta}_{q_k}^* \gamma_5 \delta_{q_k, p_n - p_m} & (\not{p}_n - \not{\mu}) \delta_{p_m, p_n} \end{pmatrix} \quad (19)$$

is the  $(p_m, p_n)$ -component of the inverse quark propagator in momentum representation. Note that in general  $S^{-1}$  is not diagonal in momentum space because the condensates  $\hat{\Delta}_{q_k}$  couple different momenta. Physically, this corresponds to processes like the absorption of a quark with momentum  $p_n$  by the condensate together with the emission of an antiquark or a hole with momentum  $p_m = p_n + q_k$ . This is only possible because the inhomogeneous diquark condensates carry momentum. In the homogeneous case,  $\hat{\Delta}(x) = \text{const.}$ , only the momentum component  $q_k = 0$  exists, and the in- and outgoing quark momenta are equal. While this is no longer true for our inhomogeneous ansatz, the fact that we consider a static solution still guarantees that the *energy* of the quark is conserved, see Eq. (12). This means,  $S^{-1}$  is still diagonal in the Matsubara frequencies  $\omega_{p_n}$ .

Since the action, Eq. (18), is bilinear in the fields (plus a field independent term) the mean field thermodynamic potential is readily evaluated. We obtain

$$\Omega_{MF}(T, \mu) = \Omega_0(T, \mu) + \frac{1}{4H} \sum_A \sum_{q_k} |\Delta_{A, q_k}|^2, \quad (20)$$

with

$$\Omega_0(T, \mu) = -\frac{1}{2} \frac{T}{V} \text{Tr} \ln \frac{S^{-1}}{T}, \quad (21)$$

where the trace is to be taken over the Nambu-Gor'kov, Dirac, color, flavor, and momentum components of the inverse propagator. The factor  $\frac{1}{2}$  in front corrects for overcounting due to the artificial doubling of the degrees of freedom in Nambu-Gor'kov formalism.

As pointed out above, the inverse propagator is diagonal in the energy components. This allows us to perform the energy trace, i.e., the Matsubara sum in the usual way. To that end we write

$$S_{p_m, p_n}^{-1} = \gamma^0 (i\omega_{p_n} - \mathcal{H}_{\vec{p}_m, \vec{p}_n}) \delta_{\omega_{p_m}, \omega_{p_n}}, \quad (22)$$

with the effective Hamilton operator

$$\mathcal{H}_{\vec{p}_m, \vec{p}_n} = \begin{pmatrix} (\gamma^0 \not{p}_n - \mu) \delta_{\vec{p}_m, \vec{p}_n} & -\sum_{\vec{q}_k} \hat{\Delta}_{q_k} \gamma^0 \gamma_5 \delta_{\vec{q}_k, \vec{p}_m - \vec{p}_n} \\ \sum_{\vec{q}_k} \hat{\Delta}_{q_k}^* \gamma_0 \gamma_5 \delta_{\vec{q}_k, \vec{p}_n - \vec{p}_m} & (\gamma^0 \not{p}_n + \mu) \delta_{\vec{p}_m, \vec{p}_n} \end{pmatrix}, \quad (23)$$

which does not depend on  $\omega_{p_n}$ . Here we have introduced the notation  $\vec{p} = \vec{\gamma} \cdot \vec{p}$ .

Since  $\mathcal{H}$  is hermitian, it can in principle be diagonalized. We can then employ the formula

$$T \sum_{\omega_{p_n}} \ln \left( \frac{i\omega_{p_n} + E_\lambda}{T} \right) = \frac{E_\lambda}{2} + T \ln \left( 1 + e^{-E_\lambda/T} \right) \quad (24)$$

to turn out the Matsubara sum. In this way we obtain

$$\Omega_0(T, \mu) = -\frac{1}{4V} \sum_\lambda \left( E_\lambda + 2T \ln \left( 1 + 2e^{-E_\lambda/T} \right) \right), \quad (25)$$

where the sum is over all eigenvalues  $E_\lambda$  of  $\mathcal{H}$  in Nambu-Gor'kov, Dirac, color, flavor, and three-momentum space.

Eq. (25) is formally the same as for homogeneous condensates. In practice, since  $\mathcal{H}$  is not diagonal in three-momentum space, its diagonalization is of course much more difficult in the inhomogeneous case. However, as a consequence of the periodicity of the crystal,  $\mathcal{H}$  can be brought into block diagonal form. As obvious from Eq. (23), only those quark momenta  $\vec{p}_m$  and  $\vec{p}_n$  are coupled which differ by a momentum  $\vec{q}_n$  belonging to the *R.L.* of the crystal. On the other hand we have seen earlier that, for a quantization volume  $V$  containing  $N^3$  unit cells, the mesh of allowed quark momenta is  $N^3$  times finer than the *R.L.*, cf. Eqs. (12) and (14). Therefore,  $\mathcal{H}$  can be decomposed into  $N^3$  independent blocks in momentum space. The sum over the eigenstates  $\lambda$  in Eq. (25) thus separates into a sum over the different blocks times a sum over the eigenstates of each block. The reader may recognize that this structure is deeply related to the Bloch theorem which basically says that eigenfunctions can be labelled by a vector in the Brillouin zone (*B.Z.*) and that eigenfunctions for different vectors are orthogonal.

More precisely, we write

$$\vec{p}_m = \vec{k}_m + \vec{q}_m, \quad \vec{p}_n = \vec{k}_n + \vec{q}_n, \quad (26)$$

where  $\vec{q}_m$  and  $\vec{q}_n$  are elements the *R.L.* and  $\vec{k}_m$  and  $\vec{k}_n$  belong to the *B.Z.* Then  $\vec{p}_m$  and  $\vec{p}_n$  are coupled only if  $\vec{k}_m = \vec{k}_n$ . For each vector  $\vec{k}_n$  in the *B.Z.* we therefore define a projector

$$\left( P_{\vec{k}_n} \right)_{\vec{p}_m, \vec{p}_n} = \sum_{\vec{q}_m, \vec{q}_n \in R.L.} \delta_{\vec{p}_m - \vec{k}_n, \vec{q}_m} \delta_{\vec{p}_n - \vec{k}_n, \vec{q}_n}, \quad (27)$$

which commutes with  $\mathcal{H}$  and which projects out the block of coupled momenta related to  $\vec{k}_n$ . The effective Hamilton operator  $\mathcal{H}$ , Eq. (23), can thus be written as a direct sum

$$\mathcal{H} = \sum_{\vec{k}_n \in B.Z.} \mathcal{H}(\vec{k}_n), \quad (28)$$

where

$$\left( \mathcal{H}(\vec{k}_n) \right)_{\vec{p}_m, \vec{p}_n} = \begin{pmatrix} (\gamma^0 \not{p}_n - \mu) \delta_{\vec{p}_m, \vec{p}_n} & -\hat{\Delta}_{p_m - p_n} \gamma^0 \gamma_5 \\ \hat{\Delta}_{p_n - p_m}^* \gamma_0 \gamma_5 & (\gamma^0 \not{p}_n + \mu) \delta_{\vec{p}_m, \vec{p}_n} \end{pmatrix} \quad (29)$$

is the non-trivial part of  $P_{\vec{k}_n} \mathcal{H}$ . Here  $\vec{p}_m$  and  $\vec{p}_n$  are restricted to the corresponding subspace.

Accordingly, we obtain for the thermodynamic potential

$$\begin{aligned} \Omega_0(T, \mu) = & \\ & - \frac{1}{4V} \sum_{\vec{k}_n \in B.Z.} \sum_{\lambda} \left( E_{\lambda}(\vec{k}_n) + 2T \ln \left( 1 + e^{-E_{\lambda}(\vec{k}_n)/T} \right) \right), \end{aligned} \quad (30)$$

where  $E_{\lambda}(\vec{k}_n)$  are the non-trivial eigenvalues of  $\mathcal{H}(\vec{k}_n)$ .

Finally, we can take the infinite volume limit,

$$\frac{1}{V} \sum_{\vec{k}_n \in B.Z.} \rightarrow \int_{B.Z.} \frac{d^3 k}{(2\pi)^3}. \quad (31)$$

We then obtain

$$\begin{aligned} \Omega_0(T, \mu) = & \\ & - \frac{1}{4} \int_{B.Z.} \frac{d^3 k}{(2\pi)^3} \sum_{\lambda} \left\{ E_{\lambda}(\vec{k}) + 2T \ln \left( 1 + e^{-E_{\lambda}(\vec{k})/T} \right) \right\}. \end{aligned} \quad (32)$$

In particular for  $T = 0$ , we have

$$\Omega_0(T = 0, \mu) = -\frac{1}{4} \int_{B.Z.} \frac{d^3 k}{(2\pi)^3} \sum_{\lambda} \left| E_{\lambda}(\vec{k}) \right|. \quad (33)$$

These formulas are of course consistent with the homogeneous case. In this limit the ‘‘reciprocal lattice’’ only consists of the point  $\vec{q} = 0$  and the  $B.Z.$  is the entire three-momentum space.

Before closing this section, let us give an interpretation of the momenta in the equations above. Inspecting the upper right Nambu-Gor’kov component in Eq. (29), we see that  $\hat{\Delta}_{p_m - p_n}$  couples an incoming hole with momentum  $\vec{p}_n$  to an outgoing particle with momentum  $\vec{p}_m$ . This means, the condensate contains a fermion pair with momenta  $-\vec{p}_n$  and  $\vec{p}_m$ , respectively. Writing  $\vec{p}_m = \vec{k} + \vec{q}_m$  and  $-\vec{p}_n = -\vec{k} - \vec{q}_n$  with  $\vec{k} \in B.Z.$  and  $\vec{q}_m, \vec{q}_n \in R.L.$ , we see that  $\vec{p}_m - \vec{p}_n$  is just the total momentum of the pair, whereas  $2\vec{k}$  is the relative momentum modulo momenta of the  $R.L.$

## C. Regularization

The above expressions for the thermodynamic potential are quartically divergent if the integral and the sum are left unconstrained. Therefore, we have to specify a regularization procedure to get a well defined result. Since later we want to compare the free energies of inhomogeneous and homogeneous solutions, it is of course crucial to regularize both cases in a consistent way.

We do not want to attach a physical meaning to the regularization scheme. Instead we think of a local theory,

which – at a given order in some power-counting scheme – can be ‘‘renormalized’’ by adding a finite number of local operators. The corresponding counter terms should be determinable in the homogeneous phase and be expressible through physical observables. As a consequence, the Ginzburg-Landau coefficients, which can be derived from the mean-field thermodynamic potential, should depend on the regularization only indirectly through physical observables, like the BCS gap at a given chemical potential.

Given these constraints, it is not obvious how to generalize a three-momentum cutoff regularization to inhomogeneous phases and as discussed in Appendix A the most naive approach of restricting the momenta  $\vec{k}$  of external and internal quarks to  $|\vec{k}| < \Lambda$  or  $k_F - \Lambda \leq |\vec{k}| \leq k_F + \Lambda$  does not meet our requirements.

We therefore suggest a Pauli-Villars-like regularization scheme, which we introduce via a proper-time regularization of the functional logarithm in the thermodynamic potential (see Eq. 21) and which does therefore not rely on homogeneous ground states.

In a first step we go back to Eqs. (21) and (22) and combine positive and negative Matsubara frequencies to get

$$\begin{aligned} T \sum_n \ln(i\omega_n - \mathcal{H}) &= \frac{T}{2} \sum_n \ln(i\omega_n - \mathcal{H})(-i\omega_n - \mathcal{H}) \\ &= \frac{T}{2} \sum_n \ln A, \end{aligned} \quad (34)$$

where  $A = \omega_n^2 + \mathcal{H}^2$  is a hermitian operator with positive eigenvalues. Next we replace the logarithm by its Schwinger proper-time representation,

$$\ln A \rightarrow - \int_0^{\infty} \frac{d\tau}{\tau} f(\tau) e^{-\tau A}, \quad (35)$$

where we introduced a blocking function  $f(\tau)$  as a regulator. Thus, our regularization scheme is defined by specifying  $f(\tau)$ .

The most simple prescription would be to put a lower bound in the proper-time variable,  $f(\tau) = \theta(\tau - 1/\Lambda^2)$ . However, as we would like to keep a structure which allows us to perform the Matsubara sum analytically, we prefer the function

$$f(\tau) = 1 - 2e^{-\tau\Lambda^2} + e^{-2\tau\Lambda^2}. \quad (36)$$

Inserting this into Eq. (35), this amounts to the replacement

$$\ln A \rightarrow \ln A - 2 \ln(A + \Lambda^2) + \ln(A + 2\Lambda^2), \quad (37)$$

and we can carry out the Matsubara sum as before. Then the regularized version of Eq. (32) reads:

$$\begin{aligned} \Omega_0(T, \mu) = & -\frac{1}{4} \int_{B.Z.} \frac{d^3 k}{(2\pi)^3} \sum_{\lambda} \\ & \times \sum_{j=0}^2 c_j \left\{ E_{\lambda,j}(\vec{k}) + 2T \ln \left( 1 + e^{-E_{\lambda,j}(\vec{k})/T} \right) \right\}, \end{aligned} \quad (38)$$

where  $c_0 = c_2 = 1$ ,  $c_1 = -2$ , and

$$E_{\lambda,j}(\vec{k}) = \sqrt{E_{\lambda}^2(\vec{k}) + j\Lambda^2}. \quad (39)$$

Eqs. (37) and (38) are reminiscent of Pauli-Villars regularization. Note, however, that according to Eq. (39) we replace the *free energies* in a Pauli-Villars-like manner, which is not exactly the same as introducing regulator particles with large masses, as in the standard Pauli-Villars regularization.

The two regulator terms generated by the blocking function Eq. (36) regularize quadratic divergencies. This is sufficient to get finite results for derivatives of the thermodynamic potential, like the quark number density  $-\frac{\partial\Omega}{\partial\mu}$  or the derivatives  $\frac{\partial\Omega}{\partial\Delta_{qk}}$ , which appear in the gap equations. On the other hand, since the unregularized thermodynamic potential is quartically divergent, it remains logarithmically divergent, even after the regularization. It should be kept in mind, however, that the thermodynamic potential is physically meaningful only up to a constant. We can therefore subtract the remaining divergency by calculating the difference to some reference point, like the ground state in vacuum or simply the normal conducting phase at some given chemical potential.

#### D. Simplified model

The general framework for the mean-field thermodynamic potential derived in Sec. II B, together with the regularization procedure suggested in Sec. II C, is one of our central results. It may serve as a starting point for extensive studies of the phase diagram of strongly interacting matter in future investigations. In most of the remainder of the present article, we will illustrate the power of our approach by numerical examples in a simplified version of our model.

##### 1. Dirac structure

In a first step, we derive an approximation to our model, which should be valid at high densities. Starting point is the effective Hamilton operator  $\mathcal{H}$ , Eq. (23). As we have discussed,  $\mathcal{H}$  is block diagonal in momentum space, and we can in fact concentrate on a single

block  $\mathcal{H}(\vec{k})$ , related to the offset momentum  $\vec{k} \in B.Z.$ , cf. Eq. (29). However, for the sake of notational brevity, we will drop the argument  $(\vec{k})$  in the following.

In order to reduce the complexity, and guided by high-density effective theory, we want to get rid of the Dirac structure in  $\mathcal{H}$ . We first note that the eigenvalue spectrum does not change under unitary transformations. Choosing

$$U = \begin{pmatrix} 1 & 0 \\ 0 & \gamma^0\gamma_5 \end{pmatrix} = -U^\dagger = -U^{-1}, \quad (40)$$

we obtain  $\mathcal{H}' = U^\dagger \mathcal{H} U$  with

$$\mathcal{H}'_{\vec{p}_m, \vec{p}_n} = \begin{pmatrix} (\gamma^0 \vec{p}_n - \mu) \delta_{\vec{p}_m, \vec{p}_n} & \hat{\Delta}_{p_m - p_n} \\ \hat{\Delta}_{p_n - p_m}^* & -(\gamma^0 \vec{p}_n + \mu) \delta_{\vec{p}_m, \vec{p}_n} \end{pmatrix}. \quad (41)$$

In homogeneous phases, a standard method to diagonalize the remaining Dirac structure is to employ energy projectors,

$$\Lambda_{\hat{p}}^\pm = \frac{1}{2}(1 \pm \gamma^0 \hat{p}), \quad (42)$$

where  $\hat{p} = \vec{p}/p$  with  $p = |\vec{p}|$ . We can then reexpress

$$\gamma^0 \vec{p}_n - \mu = (p_n - \mu) \Lambda_{\hat{p}}^+ - (p_n + \mu) \Lambda_{\hat{p}}^-, \quad (43)$$

and  $\mathcal{H}'$  can be decomposed into a positive and a negative energy part, which act on orthogonal subspaces of the Hilbert space. One can therefore find a new basis, where these positive and negative energy parts decouple.

However, as the  $\Lambda_{\hat{p}}^\pm$  are only projectors for states with the same momentum direction  $\hat{p}$ , the method described above, does not work exactly in inhomogeneous phases, where different momenta are coupled by the gap functions. In fact, we can still remove the Dirac structure from the diagonal momentum components in this way, but at the same time new Dirac structures appear in the off-diagonal components.

We can work this out explicitly by performing a unitary transformation  $\mathcal{H}'' = V^\dagger \mathcal{H}' V$  which diagonalizes the Dirac part of the diagonal momentum components  $\mathcal{H}'_{\vec{p}_m, \vec{p}_m}$ . The result reads

$$\mathcal{H}'' = \mathcal{H}''_1 + \mathcal{H}''_2, \quad (44)$$

where

$$(\mathcal{H}''_1)_{\vec{p}_m, \vec{p}_n} = \begin{pmatrix} (p_m - \mu) \delta_{\vec{p}_m, \vec{p}_n} & \hat{\Delta}_{p_m - p_n} \\ \hat{\Delta}_{p_n - p_m}^* & -(p_m - \mu) \delta_{\vec{p}_m, \vec{p}_n} \\ -(p_m + \mu) \delta_{\vec{p}_m, \vec{p}_n} & \hat{\Delta}_{p_m - p_n} \\ \hat{\Delta}_{p_n - p_m}^* & (p_m + \mu) \delta_{\vec{p}_m, \vec{p}_n} \end{pmatrix} \otimes \mathbf{1}_2 \quad (45)$$

is diagonal in Dirac space. Here we have reordered the lines and columns to make the diagonal structure obvious. The non-diagonal  $2 \times 2$  blocks now describe the Nambu-Gor'kov structure. The  $2 \times 2$  identity matrix on

the right is related to the spin degeneracy of the problem and is, thus, part of the Dirac structure.

In this basis, the remaining part of the transformed Hamiltonian is given by

$$(\mathcal{H}_2'')_{\vec{p}_m, \vec{p}_n} = \begin{pmatrix} 0 & \hat{\Delta}_{p_m-p_n} & 0 & -\hat{\Delta}_{p_m-p_n} \\ \hat{\Delta}_{p_n-p_m}^* & 0 & -\hat{\Delta}_{p_n-p_m}^* & 0 \\ 0 & -\hat{\Delta}_{p_m-p_n} & 0 & \hat{\Delta}_{p_m-p_n} \\ -\hat{\Delta}_{p_n-p_m}^* & 0 & \hat{\Delta}_{p_n-p_m}^* & 0 \end{pmatrix} \otimes \frac{1}{2} \left( (\hat{p}_m \cdot \hat{p}_n - 1) \mathbf{1}_2 + i(\hat{p}_m \times \hat{p}_n) \cdot \vec{\sigma} \right), \quad (46)$$

where  $\vec{\sigma}$  denotes the Pauli matrices, indicating a non-trivial spin structure. Obviously,  $\mathcal{H}_2''$  is not diagonal in Dirac space. However, the components of  $\mathcal{H}_2''$  vanish for parallel momenta,  $\hat{p}_m = \hat{p}_n$ . This reflects the fact that states with parallel momenta have the same energy projectors  $\Lambda_{\vec{p}}^{\pm}$ .

In the following, we will neglect  $\mathcal{H}_2''$ . We expect that this is a good approximation at very high densities where the physics is dominated by collinear scattering near the Fermi surface,  $|\vec{p}_m - \vec{p}_n| \ll p_m \sim p_n \sim \mu$ . Neglecting the antiparticle contributions as well, we obtain

$$\begin{aligned} \Omega_0(T, \mu) &= -\frac{1}{2} \int_{B.Z.} \frac{d^3 k}{(2\pi)^3} \sum_{\lambda} \left\{ E_{\lambda}(\vec{k}) + 2T \ln \left( 1 + e^{-E_{\lambda}(\vec{k})/T} \right) \right\} \\ &+ \text{regulator terms}, \end{aligned} \quad (47)$$

where  $E_{\lambda}(\vec{k})$  are now the eigenvalues of the ‘‘high-density effective Hamiltonian’’

$$(\mathcal{H}_{HDE})_{\vec{p}_m, \vec{p}_n} = \begin{pmatrix} (p_m - \mu) \delta_{\vec{p}_m, \vec{p}_n} & \hat{\Delta}_{p_m-p_n} \\ \hat{\Delta}_{p_n-p_m}^* & -(p_m - \mu) \delta_{\vec{p}_m, \vec{p}_n} \end{pmatrix} \quad (48)$$

for a given offset momentum  $\vec{k}$ .

## 2. Color-flavor structure

The second simplification concerns the color-flavor structure of the model. In Sec. II A we have chosen a form of the gap matrix which is capable to describe the most common phases in color superconductivity, see Eq. (9). For instance, the CFL phase corresponds to the case  $\Delta_2 = \Delta_5 = \Delta_7 \equiv \Delta$ .

In the following, we restrict ourselves to the 2SC pairing pattern, which is defined by  $\Delta_2 = \Delta$  and  $\Delta_5 = \Delta_7 = 0$ . Moreover, since we are only interested in the effect of the pairing relative to the normal conducting phase, we can omit those colors and flavors which do not participate in the pairing (i.e., strange quarks and, using standard

nomenclature, blue quarks). Thus, the remaining Hamiltonian is a  $4 \times 4$  matrix in color-flavor space which can trivially be decomposed into four separate blocks.

We assume that the chemical potential may be different for up and down quarks,

$$\mu_u = \bar{\mu} + \delta\mu, \quad \mu_d = \bar{\mu} - \delta\mu, \quad (49)$$

but does not depend on color. We then obtain

$$\mathcal{H}_{HDE} = \mathcal{H}_{\Delta, \delta\mu} \oplus \mathcal{H}_{-\Delta, \delta\mu} \oplus \mathcal{H}_{\Delta, -\delta\mu} \oplus \mathcal{H}_{-\Delta, -\delta\mu}, \quad (50)$$

where

$$(\mathcal{H}_{\Delta, \delta\mu})_{\vec{p}_m, \vec{p}_n} = \begin{pmatrix} (p_m - \bar{\mu} - \delta\mu) \delta_{\vec{p}_m, \vec{p}_n} & \Delta_{p_m-p_n} \\ \Delta_{p_n-p_m}^* & -(p_m - \bar{\mu} + \delta\mu) \delta_{\vec{p}_m, \vec{p}_n} \end{pmatrix}. \quad (51)$$

Of course, the eigenvalues of  $\mathcal{H}_{\Delta, \delta\mu}$  do not depend on the overall sign of  $\Delta$ . Moreover, at least in all cases to be considered in this article, replacing  $\delta\mu$  by  $-\delta\mu$  amounts to a replacement of the eigenvalue spectrum  $\{E_{\lambda}(\vec{k})\}$  by  $\{-E_{\lambda}(\vec{k})\}$  (see Appendix B). Hence, since the thermodynamic potential depends only on the moduli of the eigenvalues, each of the four blocks contributes equally, and we only need to determine the eigenvalues of  $\mathcal{H}_{\Delta, \delta\mu}$ .

## 3. Gap equations

Summarizing our main equations, including the approximations introduced above, the regularized mean-field thermodynamic potential is given by

$$\Omega(T, \bar{\mu}, \delta\mu) = \Omega_0(T, \bar{\mu}, \delta\mu) + \frac{1}{4H} \sum_{q_k} |\Delta_{q_k}|^2, \quad (52)$$

with

$$\begin{aligned} \Omega_0(T, \bar{\mu}, \delta\mu) = & -2 \int_{B.Z.} \frac{d^3k}{(2\pi)^3} \sum_{\lambda} \\ & \times \sum_{j=0}^2 c_j \left\{ E_{\lambda,j}(\vec{k}) + 2T \ln \left( 1 + e^{-E_{\lambda,j}(\vec{k})/T} \right) \right\}, \end{aligned} \quad (53)$$

where  $c_0 = c_2 = 1$ ,  $c_1 = -2$ , and  $E_{\lambda,j}(\vec{k}) = \sqrt{E_{\lambda}^2(\vec{k}) + j\Lambda^2}$  as in Eq. (39).  $E_{\lambda}(\vec{k})$  are now the eigenvalues of  $\mathcal{H}_{\Delta,\delta\mu}(\vec{k})$ , Eq. (51). At  $T = 0$ , which will be our main focus, this becomes

$$\Omega_0(T = 0, \bar{\mu}, \delta\mu) = -2 \int_{B.Z.} \frac{d^3k}{(2\pi)^3} \sum_{\lambda} \sum_{j=0}^2 c_j \left| E_{\lambda,j}(\vec{k}) \right|. \quad (54)$$

As discussed earlier, in order to get a finite result for  $\Omega$ , one still has to subtract an infinite constant. In this paper, we will always consider the free-energy difference to the normal phase, i.e., the phase with  $\Delta \equiv 0$  at the same value of  $T$ ,  $\bar{\mu}$ , and  $\delta\mu$ . This quantity is finite.

Finally, before coming to the numerical results, we want to discuss the gap equations. As in the homogeneous case we have to minimize the thermodynamic potential, which means that we have to solve the equations

$$0 = \frac{\partial\Omega}{\partial\Delta_{q_k}^*} = \frac{\partial\Omega_0}{\partial\Delta_{q_k}^*} + \frac{\Delta_{q_k}}{4H} \quad (55)$$

for all Fourier components. From Eq. (53), we obtain

$$\begin{aligned} \frac{\partial\Omega_0}{\partial\Delta_{q_k}^*} = & -2 \int_{B.Z.} \frac{d^3k}{(2\pi)^3} \sum_{\lambda} \frac{\partial E_{\lambda}}{\partial\Delta_{q_k}^*} \\ & \times \sum_{j=0}^2 c_j \left( 1 - 2n(E_{\lambda,j}) \right) \frac{E_{\lambda,j}}{E_{\lambda}}, \end{aligned} \quad (56)$$

where  $n(E) = [\exp(E/T) + 1]^{-1}$  is a Fermi function. To evaluate this further, we use that  $E_{\lambda}$  are the eigenvalues of  $\mathcal{H}_{\Delta,\delta\mu}$ . This means, there are unitary matrices  $U$  so that

$$\tilde{\mathcal{H}}_{\Delta,\delta\mu} = U^{-1} \mathcal{H}_{\Delta,\delta\mu} U \quad (57)$$

is a diagonal matrix with  $(\tilde{\mathcal{H}}_{\Delta,\delta\mu})_{\lambda\lambda} = E_{\lambda}$ . Hence,

$$\frac{\partial E_{\lambda}}{\partial\Delta_{q_k}^*} = \frac{\partial}{\partial\Delta_{q_k}^*} (U^{-1} \mathcal{H}_{\Delta,\delta\mu} U)_{\lambda\lambda} = (U^{-1} P_{q_k} U)_{\lambda\lambda}, \quad (58)$$

where  $P_{q_k} = \frac{\partial}{\partial\Delta_{q_k}^*} \mathcal{H}_{\Delta,\delta\mu}$  is a known  $\Delta$ - and  $\vec{k}$ -independent matrix (see Eq. (61) below). Note that the terms related to the derivatives of  $U^{-1}$  and  $U$  cancel each

other. Writing the matrix  $U = (w_1, \dots)$  in terms of the eigenvectors  $w_{\lambda}$  to the eigenvalues  $E_{\lambda}$ , this yields

$$\frac{\partial E_{\lambda}}{\partial\Delta_{q_k}^*} = w_{\lambda}^{\dagger} P_{q_k} w_{\lambda}. \quad (59)$$

In fact, this formula is nothing but first-order perturbation theory for the modification of the eigenvalues under a small perturbation  $\delta\mathcal{H}_{\Delta,\delta\mu} = P_{q_k} \delta\Delta_{q_k}$ . If we insert this into Eq. (56), we can then rewrite Eq. (55) into the gap equations

$$\begin{aligned} \Delta_{q_k} = & 8H \int_{B.Z.} \frac{d^3k}{(2\pi)^3} \sum_{\lambda} w_{\lambda}^{\dagger} P_{q_k} w_{\lambda} \\ & \times \sum_{j=0}^2 c_j \left( 1 - 2n(E_{\lambda,j}) \right) \frac{E_{\lambda,j}}{E_{\lambda}}. \end{aligned} \quad (60)$$

These equations are the basis for our numerical analysis.

At this point, we would like to note that the matrix  $P_{q_k}$  connects momenta differing by  $\vec{q}_k$ . In fact, from Eq. (51) we get

$$(P_{q_k})_{\vec{p}_m, \vec{p}_n} = \begin{pmatrix} 0 & 0 \\ 1 & 0 \end{pmatrix} \delta_{\vec{p}_n - \vec{p}_m, \vec{q}_k}. \quad (61)$$

Thus, denoting the Nambu-Gor'kov components of the eigenvectors as  $w_{\lambda} = (u_{\lambda}, v_{\lambda})$  and indicating the momentum components explicitly, the gap equations read

$$\Delta_{q_k} = 8H \int_{B.Z.} \frac{d^3k}{(2\pi)^3} \sum_{\lambda, \vec{p}_n} (v_{\lambda}^{\dagger})_{\vec{p}_n - \vec{q}_k} (u_{\lambda})_{\vec{p}_n} \left( 1 - 2n(E_{\lambda}) \right), \quad (62)$$

where we have omitted the regulator terms for simplicity. Fourier transforming this convolution with the conventions given in Eqs. (11,13) we get

$$\Delta(x) = 8HV \int_{B.Z.} \frac{d^3k}{(2\pi)^3} \sum_{\lambda} v_{\lambda}^{\dagger}(x) u_{\lambda}(x) \left( 1 - 2n(E_{\lambda}) \right), \quad (63)$$

where  $V$  is the volume of the unit cell. This is precisely the selfconsistency condition for the Bogoliubov-de Gennes equation [38] when again exploiting Bloch's theorem. It is obvious that this relation is not restricted to the simplified model we discussed here, but an extension to the general case is straight forward. Note however that our regularization procedure and therefore also our numerical calculations are tied in momentum space.

### III. NUMERICAL RESULTS

In this section we want to discuss numerical calculations performed within the simplified model of Sec. II D. We restrict ourselves to  $T = 0$  and to a fixed average chemical potential  $\bar{\mu} = 400$  MeV. Then  $\delta\mu$  is the only remaining external variable and we will drop the arguments  $T$  and  $\bar{\mu}$  in the following.



Our model has two parameters, namely the coupling constant  $H$  and the cutoff parameter  $\Lambda$ . We remind that  $\Lambda$  restricts the free energies and not the momenta. Thus, the most relevant excitations around the Fermi surface are always included, and there is no need for  $\Lambda$  to be larger than the chemical potential. Of course,  $\Lambda$  should be considerably larger than the gap. Having fixed the cutoff, we will express the coupling constant  $H$  through the corresponding value of the BCS gap.

For given model parameters and  $\delta\mu$ , the thermodynamic potential, as defined above, depends on the gap function  $\Delta$ . Our main goal is to find the most stable solution, i.e., the minimum of  $\Omega$  with respect to  $\Delta$ . At a given periodicity of the crystal, this corresponds to minimizing  $\Omega$  with respect to the Fourier components  $\Delta_{q_k}$ , i.e., to finding the most favored solution of the coupled set of gap equations, Eq. (60). In addition, we should vary the periodic structure itself, i.e., the basis vectors of the reciprocal lattice. Obviously, this is a very involved problem, which is beyond the scope of the present paper.

Therefore, as a first step, we restrict ourselves to one-dimensional crystalline structures, i.e., to gap functions which vary periodically in one spatial direction  $\hat{q}$ , but stay constant in the two spatial directions perpendicular to  $\hat{q}$ . Moreover, we only consider real gap functions. In spite of these restrictions, we find an interesting class of solutions, which will be discussed in Sec. III C and thereafter. First, however, we briefly discuss the BCS and the Fulde-Ferrell solutions within our model in order to provide a basis and to make contact to the literature.

### A. BCS phase

The BCS solution corresponds to the limit of spatially homogeneous condensates. In this case the Brillouin zone is the entire three-dimensional space and we have

$$\Delta_{q_k} = \Delta \delta_{q_k,0}. \quad (64)$$

Therefore, the effective Hamiltonian Eq. (51) is diagonal in momentum space, and we obtain the eigenvalues

$$|E_{\pm}(\vec{k})| = |\sqrt{(k - \bar{\mu})^2 + |\Delta|^2} \pm \delta\mu|. \quad (65)$$

Inserting this into Eqs. (52) and (54) we recover the well-known result that for  $\delta\mu < |\Delta|$  the *unregularized* part of the thermodynamic potential,

$$\Omega_{unreg}(\delta\mu) = -4 \int \frac{d^3k}{(2\pi)^3} \sqrt{(k - \bar{\mu})^2 + |\Delta|^2} + \frac{|\Delta|^2}{4H}, \quad (66)$$

is independent of  $\delta\mu$  [12]. When the Pauli-Villars regulators are included, this does no longer hold exactly. As a consequence, the value of  $\Delta$  which solves the gap equation  $\partial\Omega/\partial\Delta^* = 0$  is weakly  $\delta\mu$  dependent. For this reason we *define*  $\Delta_{BCS}$  to be the gap at  $\delta\mu = 0$ . For  $\Delta_{BCS} = 80$  MeV and  $\Lambda = 400$  MeV, which will be our standard choice of parameters, we then find that  $\Delta$  increases by about five percent, when  $\delta\mu$  is varied between

0 and  $0.8 \Delta_{BCS}$ . (Higher values of  $\delta\mu$  are irrelevant for the BCS phase, as we will see below.) For smaller gaps or larger values of the cutoff the effect is even smaller.

When  $\delta\mu$  is increased, the BCS phase eventually becomes unfavored against the normal phase. The corresponding phase transition is first order. In the weak-coupling limit it occurs at  $\delta\mu = \Delta_{BCS}/\sqrt{2}$ , as shown already in 1962 by Chandrasekhar and Clogston [22]. For stronger couplings, the BCS phase can sustain somewhat larger values of  $\delta\mu$ . We will come back to this in the following subsection.

### B. Fulde-Ferrell solutions

The FF phase corresponds to the case that the gap function is a single plane wave,

$$\Delta(x) = \Delta e^{2i\vec{q}\cdot\vec{x}}. \quad (67)$$

This means, the *B.Z.* is infinite in the directions perpendicular to  $\vec{q}$ , but finite in  $\vec{q}$ -direction with length  $2|\vec{q}|$ . The momentum space representation of the gap matrix is given by

$$\Delta_{q_k} = \Delta \delta_{\vec{q}_k, 2\vec{q}}. \quad (68)$$

Inserting this into Eq. (51) one finds that the effective Hamiltonian is still block diagonal, however with shifted blocks where two momenta are coupled. These blocks can be written in the form

$$\begin{pmatrix} k_+ - \bar{\mu} - \delta\mu & \Delta \\ \Delta^* & -k_- + \bar{\mu} - \delta\mu \end{pmatrix}, \quad (69)$$

with  $k_{\pm} = |\vec{k} \pm \vec{q}|$ . Moreover, the sum over all blocks simply amounts to extending the  $\vec{k}$ -integration to the entire space. Hence, the thermodynamic potential reads

$$\Omega(\delta\mu) = -2 \int \frac{d^3k}{(2\pi)^3} \sum_{\lambda=\pm} (|E_{\lambda}(\vec{k})| + \text{reg.}) + \frac{|\Delta|^2}{4H}, \quad (70)$$

where

$$E_{\pm}(\vec{k}) = \frac{k_+ - k_-}{2} \pm \sqrt{\left(\frac{k_+ + k_-}{2} - \bar{\mu}\right)^2 + |\Delta|^2} - \delta\mu \quad (71)$$

are the eigenvalues of the matrix (69). Apart from the Pauli-Villars regulators in Eq. (70), this is again a standard result.

In order to find the most favored FF solution, we must minimize the thermodynamic potential with respect to  $|\Delta|$  and  $|\vec{q}|$ . Typically, one finds that  $|\vec{q}|$  is of the order of  $0.9 \Delta_{BCS}$  while  $|\Delta|$  is considerably smaller than  $\Delta_{BCS}$ .<sup>1</sup> Numerical examples for  $\Delta_{BCS} = 80$  MeV and

<sup>1</sup> In the weak-coupling limit,  $|\vec{q}| = 0.906 \Delta_{BCS}$  and  $|\Delta| = 0.23 \Delta_{BCS}$  at the Chandrasekhar-Clogston point [1, 2].

$\Lambda = 400$  MeV will be discussed in the context of Figs. 5 and 6.

In competition with the normal phase and the BCS phase, this optimal FF solution is favored only in a small window in  $\delta\mu$ . This is shown in Fig. 1, where the phase boundaries are displayed as functions of  $\Delta_{BCS}$  for two different values of the cutoff. The phase transitions are of first order for the BCS-FF transition (dashed lines) and of second order for the FF-normal transition (solid lines). Indeed, in the weak-coupling limit, one expects a first-order phase transition from the BCS phase to the FF phase near the Chandrasekhar-Clogston value  $\delta\mu = \Delta_{BCS}/\sqrt{2}$  followed by the second-order phase transition to the normal phase at  $\delta\mu = 0.754 \Delta_{BCS}$  [1, 2]. These values are indicated in the figure by the thin horizontal lines. Obviously, the model results come close to these limits for  $\Delta_{BCS} \rightarrow 0$ , whereas for stronger interactions we again find deviations.

The BCS-FF phase boundaries are almost identical with the corresponding BCS-normal boundaries because the free energy difference between BCS phase and normal phase is a much steeper function of  $\delta\mu$  than the free energy difference between FF phase and normal phase (see Fig. 4). This is a standard result, which was also found, e.g., in Ref. [32] where a different regularization scheme was used.

The FF-normal phase boundary, on the other hand, behaves rather differently from the result of Ref. [32]. There, it was found that the critical  $\delta\mu$  decreases with increasing  $\Delta_{BCS}$ . As a consequence, the BCS-FF boundary and the FF-normal boundary intersect at some  $\Delta_{BCS} \sim 100$  MeV, and there is no stable FF solution at stronger couplings. In contrast to this, we find that the FF-normal phase boundary runs almost parallel to the BCS-FF phase boundary so that the width of the FF window stays approximately constant. This means, as long as we do not consider other inhomogeneous phases, the regime of stable FF solutions extends to very large values of  $\Delta_{BCS}$  in our regularization scheme.

### C. General solutions for real one-dimensional gap functions

We now turn to the main part of this work, being the analysis of ground states when allowing for a real one-dimensional gap function as the order parameter. For simplicity, we will often call these solutions “general solutions”, although there should be, of course, even more general solutions with higher-dimensional or complex gap functions.

In the first step we limit ourselves to periodic gap functions of the form

$$\Delta(x) = \sum_k \Delta_{\vec{q},k} e^{2ik\vec{q}\cdot\vec{x}}. \quad (72)$$

For each period given through  $|\vec{q}|$  we will then minimize the thermodynamic potential with respect to the Fourier

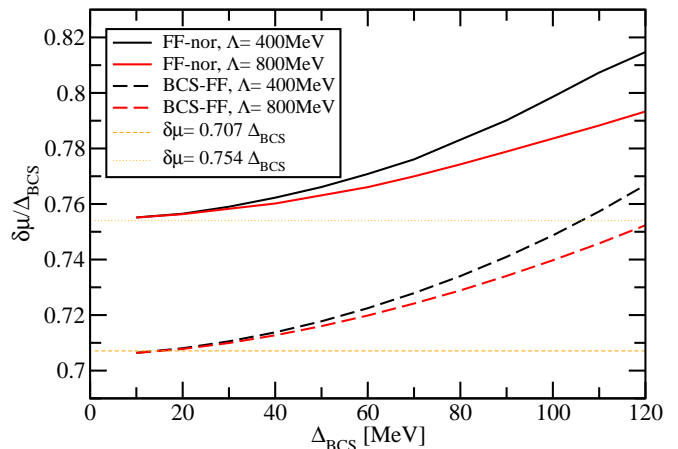


FIG. 1: Stability window in  $\delta\mu$  for the FF phase in competition with the BCS phase and the normal phase as a function of the coupling, parameterized by  $\Delta_{BCS}$ . The BCS phase is favored below the dashed lines, the normal phase is favored above the solid lines. Results for two different cutoffs are shown. The thin horizontal lines indicate the weak-coupling limits.

components  $\Delta_{\vec{q},k}$  and afterwards with respect to  $|\vec{q}|$ .

Comparing Eq. (72) with Eqs. (11) and (12), we find that  $\vec{q}_k = 2k\vec{q}$ . The (admittedly somewhat unnatural) factor of 2 was introduced to give  $\vec{q}$  the same meaning as in the FF ansatz, Eq. (67), where this factor is the standard convention.

Again the  $B.Z.$  is infinite in the directions perpendicular to  $\vec{q}$  and finite in the  $\vec{q}$ -direction with length  $2|\vec{q}|$ . Without loss of generality, we can assume that  $\vec{q}$  points in  $z$ -direction,  $\vec{q} = q\vec{e}_z$ . Then one period corresponds to  $z = \frac{\pi}{q}$ .

The restriction to gap functions which are real in coordinate space means that the Fourier components satisfy the relation  $\Delta_{\vec{q},k} = \Delta_{\vec{q},-k}^*$ . Moreover, without loss of generality, we can always choose the origin to be located at a maximum of the gap function.  $\Delta(z)$  is then an even<sup>2</sup> function, and the Fourier components are real.

In the following we fix the model parameters to  $\Lambda = 400$  MeV and a coupling strength corresponding to  $\Delta_{BCS} = 80$  MeV. As before, we consider  $T = 0$  and  $\bar{\mu} = 400$  MeV.

In Fig. 2 we present examples of one-dimensional gap functions  $\Delta(z)$  we obtained by minimizing the thermodynamic potential at  $\delta\mu = 0.7\Delta_{BCS}$  for different fixed periods. For convenience,  $z$  is measured in units of  $\pi/\Delta_{BCS}$  so that one period is given by  $(q/\Delta_{BCS})^{-1}$ . At  $q \sim \Delta_{BCS}$

<sup>2</sup> In our numerical analysis, we only found solutions which are symmetric under reflections at a plane perpendicular to  $\vec{q}$  going through a maximum or minimum. So far, we cannot exclude that other solutions exist which do not have this symmetry. In this case  $\Delta(z)$  would of course not be an even function.

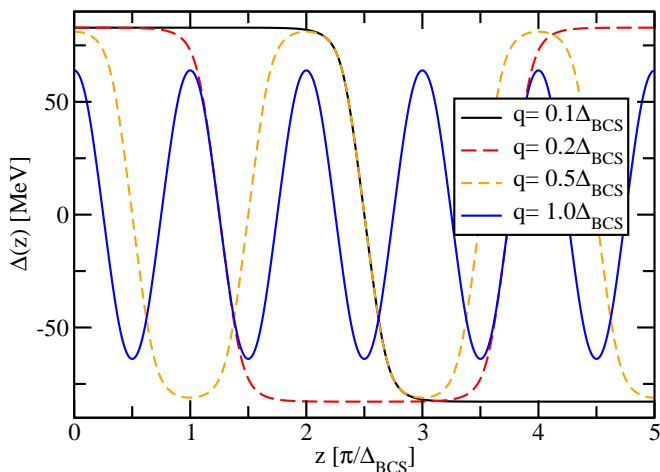


FIG. 2: The gap function in coordinate space at  $\delta\mu = 0.7\Delta_{BCS}$  for different fixed values of  $q$ .

the gap function appears to be sinusoidal. For larger periods, however, a new feature becomes apparent: the formation of a soliton lattice. Especially for  $q = 0.1\Delta_{BCS}$ , we see that the gap function stays nearly constant at  $\pm\Delta_{BCS}$  for about one half-period and then changes its sign in a relatively small interval. The  $q = 0.2\Delta_{BCS}$  solution behaves qualitatively similar, but has a shorter plateau. Remarkably, the shape of the two functions is almost identical in the transition region where the gap functions change sign. This remains even true for the  $q = 0.5\Delta_{BCS}$  solution, which is kind of an extreme case with no plateau and only transition regions. We may thus interpret these transition regions as very weakly interacting solitons, which are almost unaffected by the presence of the neighboring (anti-) solitons as long as they do not overlap.

These features will be discussed in more detail in Sec. III E. The main result is that the gap functions are characterized by two independent scales. The first scale,  $q$ , determines the period of the lattice and thereby the distance between the solitons. The second scale,  $\Delta_{BCS}$ , is not only the amplitude but also determines the shape of the solitons, which is practically independent of  $q$ . In fact, even for the sinusoidal solution at  $q = \Delta_{BCS}$ , the slope at the zero crossing is almost the same as for the  $q = 0.1\Delta_{BCS}$  solution, although the period differs by one order of magnitude.

For each  $\delta\mu$ , with the solutions for the different chosen values of  $q$  at hand, we now have to minimize the thermodynamic potential in  $q$  in order to determine the energetically preferred ground state. This is illustrated in Fig. 3, where the difference  $\delta\Omega$  between the thermodynamic potential of the inhomogeneous phase and the normal phase is displayed as a function of  $q$  for three different values of  $\delta\mu$ . We observe that the preferred value of  $q$  rises from small values towards  $\Delta_{BCS}$  when increasing  $\delta\mu$ . Also the shape of the potential changes.

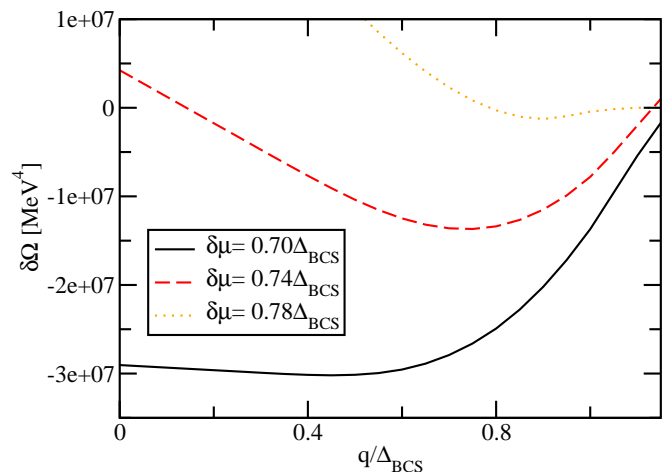


FIG. 3: Difference between the thermodynamic potentials of the general inhomogeneous phase and the normal phase as a function of  $q$  for different values of  $\delta\mu$ .

We want to point out that the BCS phase is included in this plot as  $q = 0$ . It is interesting to note that the inhomogeneous phase is the preferred phase already at  $\delta\mu = 0.70\Delta_{BCS}$ , i.e., significantly below the transition between the BCS phase and the FF phase (cf. Fig. 1).

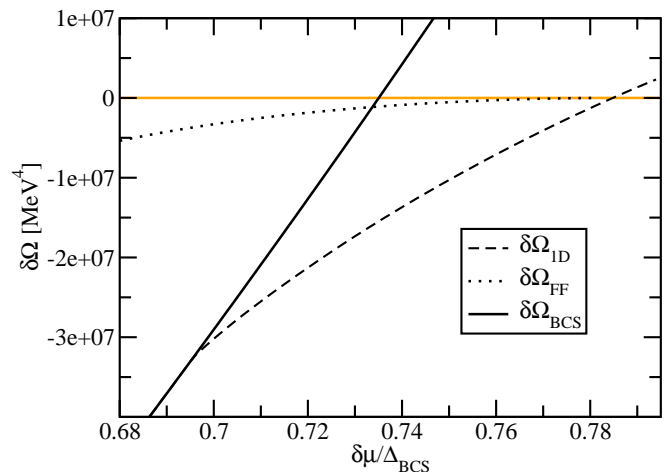


FIG. 4: Difference between the thermodynamic potentials of different phases and the normal phase as functions of  $\delta\mu$ : BCS phase (solid line), general inhomogeneous phase (dashed line), and FF phase (dotted line).

This is also seen in Fig. 4, where  $\delta\Omega$  is displayed as a function of  $\delta\mu$  for the general solution in comparison with the BCS phase and the FF phase. The shown results for the inhomogeneous phases correspond to the preferred values of  $q$  at each  $\delta\mu$ . We find that the LOFF window, i.e., the interval of  $\delta\mu$  for which a general inhomogeneous ground state is energetically favored, has almost doubled compared to the FF window. This is due to the fact that the interval is expanded towards smaller values of  $\delta\mu$ , the

upper end is almost unchanged. Related to this, the free energy gain of the general solution is much larger than that of the FF phase.

However, the most striking features which are visible in Fig. 4 are the orders of the phase transitions. Whereas for the FF solutions, the phase transition to the BCS phase is first order and to the normal phase is second order, it is just the other way around for the general inhomogeneous solutions: Here we find a first-order phase transition to the normal phase, whereas the transition to the BCS phase at the lower end appears to be continuous.

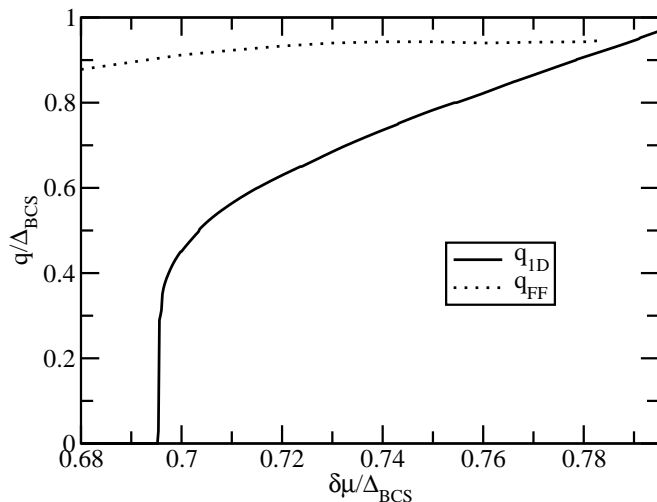


FIG. 5: The energetically preferred value of  $q$  in the general inhomogeneous superconducting phase (solid) and for the FF solutions (dotted) as functions of  $\delta\mu$ . The solution for the FF phase stops at the transition to the normal phase.

The latter is possible because our space of possible solutions allows for a natural connection between these phases via the formation of a soliton lattice. This becomes more clear in Fig. 5 where the energetically favored values of  $q$  are displayed as functions of  $\delta\mu$ . The solid line and the dotted line correspond to the general inhomogeneous phase and to the FF phase, respectively. In the FF phase,  $q$  is always of the order of  $\Delta_{BCS}$ . Similar values of  $q$  are also found for the general solutions in the upper part of the LOFF window,  $\delta\mu \gtrsim 0.75\Delta_{BCS}$ . With decreasing  $\delta\mu$ , however, the preferred  $q$  decreases to arbitrarily small values and eventually goes to zero at  $\delta\mu \approx 0.695\Delta_{BCS}$ .

We thus arrive at the following picture: With lowering  $\delta\mu$ , the period of the gap function increases and we eventually obtain a soliton lattice with increasing distance between the solitons, i.e., with constant plateaus of increasing length, see Fig. 2. At the critical point, the length of the plateaus diverges, and the inhomogeneous phase is continuously connected to the BCS phase. Also notice that, although the transition is continuous, the slope of the function  $q(\delta\mu)$  changes dramatically when  $q/\Delta_{BCS}$  comes to the order of 0.5. As we have seen in Fig. 2, this is just the regime, where the more sinusoidal solutions go over into a soliton lattice.

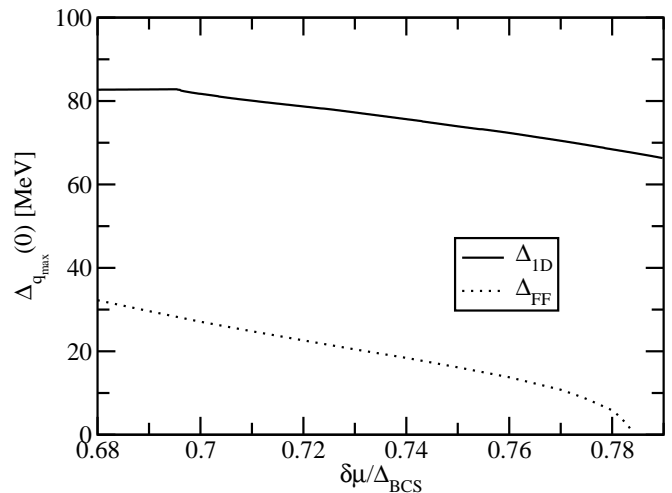


FIG. 6: The amplitude of the gap function  $\Delta(z)$  at the energetically preferred value of  $q$  at given  $\delta\mu$  for the general inhomogeneous phase (solid line) and the FF phase (dotted line).

In Fig. 6 the amplitude of the general inhomogeneous gap function is displayed as a function of  $\delta\mu$  (solid line). Since the transition to the BCS phase is continuous, the amplitude becomes equal to the BCS gap at the lower end of the window.<sup>3</sup> With increasing  $\delta\mu$ , the amplitude decreases, but it remains of the order of  $\Delta_{BCS}$  in the entire interval. For comparison, we also show the amplitude of the FF solution (dotted line). In contrast to the general solution it is always considerably smaller than  $\Delta_{BCS}$  and goes to zero at the transition point to the normal phase. Thus, in agreement with our conclusions from Fig. 4, the transition to the normal phase is of second order for the FF phase, but first order for the general inhomogeneous phase. The fact that the amplitude of the general solution is considerably bigger than the amplitude in the FF phase also reflects our earlier observation that the general solution is energetically much more favored (see Fig. 4).

At first sight, a first-order phase transition from the inhomogeneous phase to the normal phase seems to be in contradiction with Ginzburg-Landau investigations. As already discussed in the context of Figs. 2 and 5 and as will be detailed in section III E, the shape of the gap function becomes more and more sinusoidal with increasing  $\delta\mu$ , i.e., increasing  $q$ . A sinusoidal (or so-called antipodal) gap function has been investigated in a Ginzburg-Landau analysis, showing that the transition from the inhomogeneous phase to the normal phase is of second order [31, 34]. Since in the vicinity of a second-order transition the Ginzburg-Landau approximation is expected to converge to the exact mean-field result, an explanation

<sup>3</sup> We remind that, because of the regularization terms, the BCS gap at  $\delta\mu > 0$  is slightly larger than  $\Delta_{BCS}$ .

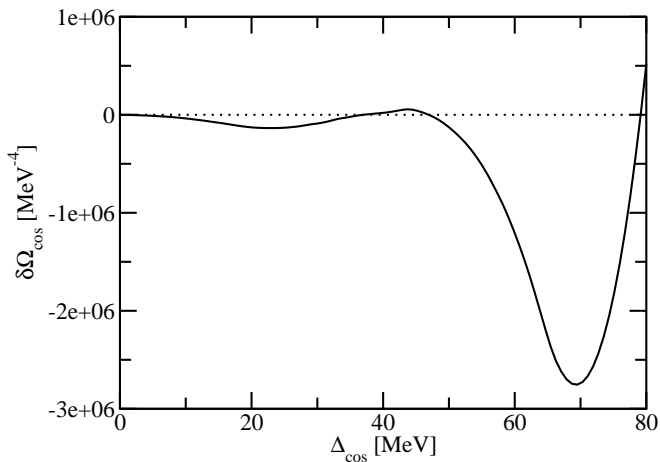


FIG. 7: Difference between the thermodynamic potential of an inhomogeneous phase with a sinusoidal gap function and the normal phase as a function of the magnitude of the gap function. Here we have chosen  $q = 0.9\Delta_{BCS}$  and  $\delta\mu = 0.775\Delta_{BCS}$ .

of this discrepancy is needed.

To clarify this issue, we determine the thermodynamic potential for a gap function

$$\Delta(z) = \Delta_{\text{cos}} \cos(2qz) \quad (73)$$

with fixed  $q$ , as being used in the Ginzburg-Landau analysis. An example is shown in Fig. 7, which corresponds to  $q = 0.9\Delta_{BCS}$  and  $\delta\mu = 0.775\Delta_{BCS}$ . We see that the thermodynamic potential has two minima in this subset of possible solutions. The more shallow one at lower magnitudes of  $\Delta_{\text{cos}}$  may be described by the Ginzburg-Landau analysis. However, in order to get the second minimum, one needs at least to include terms of the order  $\Delta_{\text{cos}}^8$ , whereas in Refs. [31, 34] at most terms of the order  $\Delta_{\text{cos}}^6$  were included. Moreover, investigations in one spatial dimension have revealed that a gradient expansion of the thermodynamic potential may even not exist at all [48]. Therefore it is unclear whether the second minimum is determinable in a Ginzburg-Landau approach, even if higher powers in the order parameter are included.

#### D. Quasiparticle spectrum

Next we want to discuss the excitation spectrum of the quasiparticles and its impact on the shape of the energetically preferred gap functions. For a given vector  $\vec{k}$  in the  $B.Z.$  we have a discrete eigenvalue spectrum of the associated Hamiltonian  $\mathcal{H}_{\Delta,\delta\mu}(\vec{k})$ , Eq. (51), which depends on  $\vec{k}$  via its allowed momenta, see Eqs. (26-29). As the inhomogeneous gap functions break the rotational symmetry of the system, this eigenvalue spectrum does not only depend on the modulus of  $\vec{k}$ , but also on its direction. Therefore, we will present the spectrum by showing selected slices through the  $B.Z.$

We note that the eigenvalue spectrum of  $\mathcal{H}_{\Delta,\delta\mu}$  depends on  $\delta\mu$  in two ways: First, there is an explicit  $\delta\mu$  term in the diagonal Nambu-Gor'kov components and, second, there is an implicit  $\delta\mu$  dependence through the  $\delta\mu$  dependence of the gap functions. For fixed gap functions, the explicit  $\delta\mu$  terms simply shift the eigenvalues of  $\mathcal{H}_{\Delta,0}$  by  $-\delta\mu$ . We will therefore take this trivial effect out and show the eigenvalue spectrum of  $\mathcal{H}_{\Delta,0}$ , which we will denote by  $E_{\lambda}^{(0)}(\vec{k})$ . This spectrum then still depends on  $\delta\mu$  through the gap functions. The gap functions, in turn, depend on  $\delta\mu$  mainly through the variation of  $|\vec{q}|$  (see Figs. 2 and 5). Therefore, we present the spectra at fixed values of  $|\vec{q}|$ . As we will see below, the remaining  $\delta\mu$  dependence is very weak, i.e., the spectra are quite generic.

In Fig. 8 we show two examples of the excitation spectrum at a fixed value of the momentum  $k_{\perp}$  perpendicular to  $\vec{q}$  as a function of the momentum  $k_z$  along the direction of  $\vec{q}$ . For a real gap function, the eigenvalue spectrum possesses two symmetries: First, as shown in Appendix B, the eigenvalues  $E_{\lambda}^{(0)}$  at given momentum  $\vec{k}$  in the  $B.Z.$  appear in pairs  $(E_{\lambda}^{(0)}, -E_{\lambda}^{(0)})$ . Second, the eigenvalue spectrum at  $k_z$  and  $2|\vec{q}| - k_z$  coincide. This is related to the fact that the gap functions are even functions in  $z$ , i.e., parity is unbroken by the condensate.<sup>4</sup>

In the left panel of Fig. 8 we show the spectrum for  $k_{\perp} = 0$ . We see that there are four low-lying excitations with free energies well below  $\Delta_{BCS}$ . These modes are related to each other by the symmetries discussed above, i.e., there is in fact only one non-trivial solution at low energies. This feature is also known from analytical investigations in one spatial dimension and is related to the soliton [42]. In addition to these modes, there are (infinitely many) other excitations with higher free energies. These higher-lying modes are clearly separated from the low-lying ones, i.e., there is a gap in the excitation spectrum, at least as long as we keep  $k_{\perp}$  fixed.<sup>5</sup> In contrast to the BCS phase, the gap does, however, not start at vanishing free-energies.

The right panel of Fig. 8 corresponds to  $k_{\perp} = \bar{\mu} = 400$  MeV. Most features of this spectrum are the same as in the previous example. The main difference is the fact that now the low-lying excitation does not change its sign when  $k_z$  is varied. As a consequence, the positive and the negative solutions do not cross and there is an additional gap around vanishing free energies.

<sup>4</sup> This statement holds for our particular choice of the coordinate system. More generally, the gap functions are symmetric under reflection at a plane perpendicular to  $\vec{q}$  going through a maximum or minimum. See also footnote 2.

<sup>5</sup> We remind that here we are discussing the eigenvalue spectrum  $E_{\lambda}^{(0)}(\vec{k})$  of  $\mathcal{H}_{\Delta,\delta\mu=0}$ . The true spectrum of  $\mathcal{H}_{HDE}$  is obtained by shifting the results by  $\delta\mu$  upwards and downwards, see Eq. (50). The gap may then disappear in some cases. This is, however, irrelevant for the discussion later on in this section, which is based on the existence of a gap in the spectrum of  $\mathcal{H}_{\Delta,0}$ .

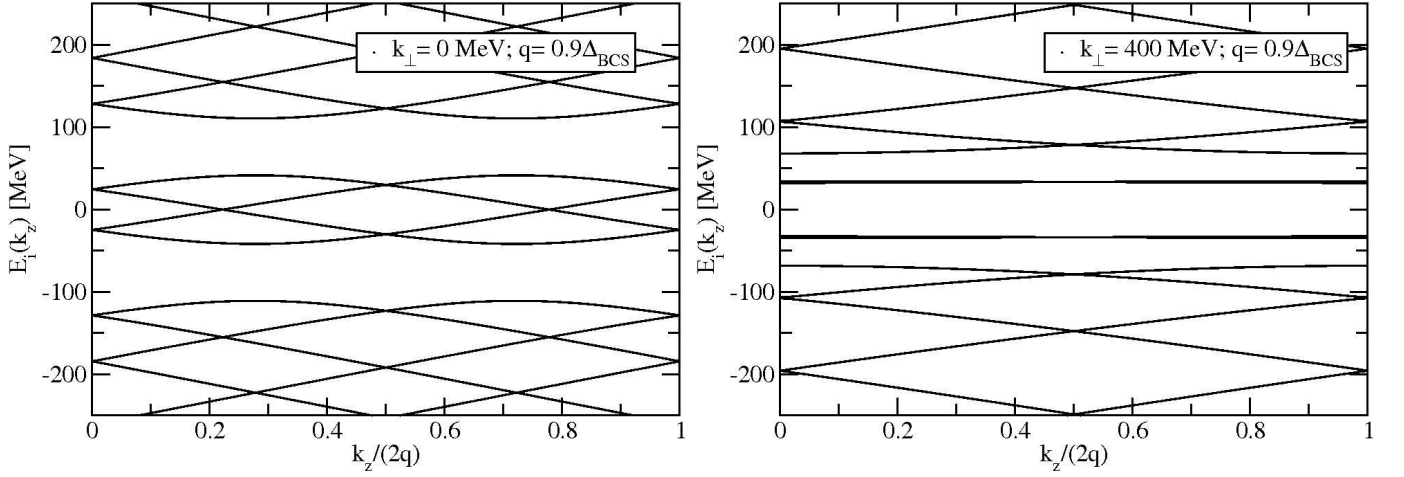


FIG. 8: Excitation spectrum in the *B.Z.* as a function of the momentum  $k_z$  parallel to  $\vec{q}$  for fixed perpendicular momentum  $k_\perp = 0$  (left panel) and  $k_\perp = 400$  MeV (right panel). Shown are the eigenvalues  $E_\lambda^{(0)}(\vec{k})$  of  $\mathcal{H}_{\Delta, \delta\mu=0}$  for the gap functions of the energetically preferred ground state at fixed  $|\vec{q}| = 0.9 \Delta_{BCS}$  and  $\delta\mu = 0.7 \Delta_{BCS}$ . The spectrum  $E_\lambda(\vec{k})$  of  $\mathcal{H}_{HDE}$  is obtained by shifting the lines by  $\delta\mu$  and  $-\delta\mu$ .

The gap structure as a function of  $k_\perp$  is visualized in Fig. 9 for two examples. The shaded areas indicate the free energies which can be reached by at least one mode at the given value of  $k_\perp$ , when  $k_z$  is varied over all possible values. Accordingly, the white areas correspond to the gapped regions. We see again that such gaps exist in the excitation spectra when  $k_\perp$  is kept fixed. There is, however, no gap when all values of  $k_\perp$  are considered.

The left panel of Fig. 9 corresponds to  $|\vec{q}| = 0.9 \Delta_{BCS}$ , i.e., to the same period as the examples shown in Fig. 8. Again, we see that the low-lying modes are restricted to a single band around zero free energies for lower values of  $k_\perp$ , whereas at higher values of  $k_\perp$  this band splits into two. Comparing this with the right panel of Fig. 9, corresponding to  $|\vec{q}| = 0.2 \Delta_{BCS}$ , we see that these features remain qualitatively unchanged. However, we observe that the bands of the low-lying modes get squeezed considerably when going from larger to smaller values of  $|\vec{q}|$ , i.e., when separating the solitons by stretching the lattice. In fact, we expect that in the limit  $|\vec{q}| \rightarrow 0$  and at low values of  $k_\perp$ , the modes associated with the soliton are restricted to exactly zero free energy, whereas the continuum starts at  $|E| = \Delta_{BCS}$ .

A gap in the complete excitation spectrum has important consequences for the dependence of the thermodynamic potential and the gap functions on  $\delta\mu$ : Consider the eigenvalues  $E_\lambda^{(0)}(\vec{k})$  of the unshifted Hamiltonian  $\mathcal{H}_{\Delta, \delta\mu=0}(\vec{k})$ . Then, as pointed out above, the eigenvalues of  $\mathcal{H}_{\Delta, \delta\mu}$  are simply given by  $E_\lambda = E_\lambda^{(0)} - \delta\mu$ . Thus, since the  $E_\lambda^{(0)}$  always come in pairs  $(E_\lambda^{(0)}, -E_\lambda^{(0)})$ , we get from Eq. (54)

$$\Omega_0(\delta\mu) = -2 \int_{B.Z.} \frac{d^3k}{(2\pi)^3} \sum_{E_\lambda^{(0)} > 0} \left( |E_\lambda^{(0)} - \delta\mu| + |E_\lambda^{(0)} + \delta\mu| \right), \quad (74)$$

where we have dropped the regularization terms for simplicity. This can be written as

$$\Omega_0(\delta\mu) = \Omega_0^{(1)} + \Omega_0^{(2)}(\delta\mu), \quad (75)$$

with a  $\delta\mu$  independent part

$$\Omega_0^{(1)} = -4 \int_{B.Z.} \frac{d^3k}{(2\pi)^3} \sum_{E_\lambda^{(0)} > \delta\mu} |E_\lambda^{(0)}(\vec{k})| \quad (76)$$

and a  $\delta\mu$  dependent part

$$\begin{aligned} \Omega_0^{(2)}(\delta\mu) &= -4 \int_{B.Z.} \frac{d^3k}{(2\pi)^3} \sum_{0 < E_\lambda^{(0)} < \delta\mu} \delta\mu \\ &\equiv -4 \delta\mu \int_{B.Z.} \frac{d^3k}{(2\pi)^3} N_s(\vec{k}) \equiv -4 \delta\mu n_s. \end{aligned} \quad (77)$$

Here  $N_s(\vec{k})$  is the number of positive eigenvalues  $E_\lambda^{(0)}(\vec{k})$  smaller than  $\delta\mu$ .

Now suppose, there was a complete gap in the spectrum in some energy interval, so that  $N_s(\vec{k})$  is constant for all values of  $\vec{k}$ , when  $\delta\mu$  is varied within this gapped interval. If  $n_s = 0$ , i.e., if  $\delta\mu$  is smaller than the smallest positive eigenvalue, the thermodynamic potential and, hence, the gap function are obviously  $\delta\mu$  independent. For  $n_s > 0$ , on the other hand, the thermodynamic potential is  $\delta\mu$  dependent. However, even in this case, the *gap functions* are still  $\delta\mu$  independent, when  $\delta\mu$  is varied within the gapped interval. This can be inferred from the gap equations,  $\frac{\delta\Omega}{\delta\Delta_{\vec{q},k}} = 0$ . A  $\delta\mu$  dependence of the gap

function must then be due to the variation  $\frac{\delta\Omega_0^{(2)}}{\delta\Delta_{\vec{q},k}}$ , because all other terms are  $\delta\mu$  independent. On the other hand, an infinitesimal variation of the gap function can only

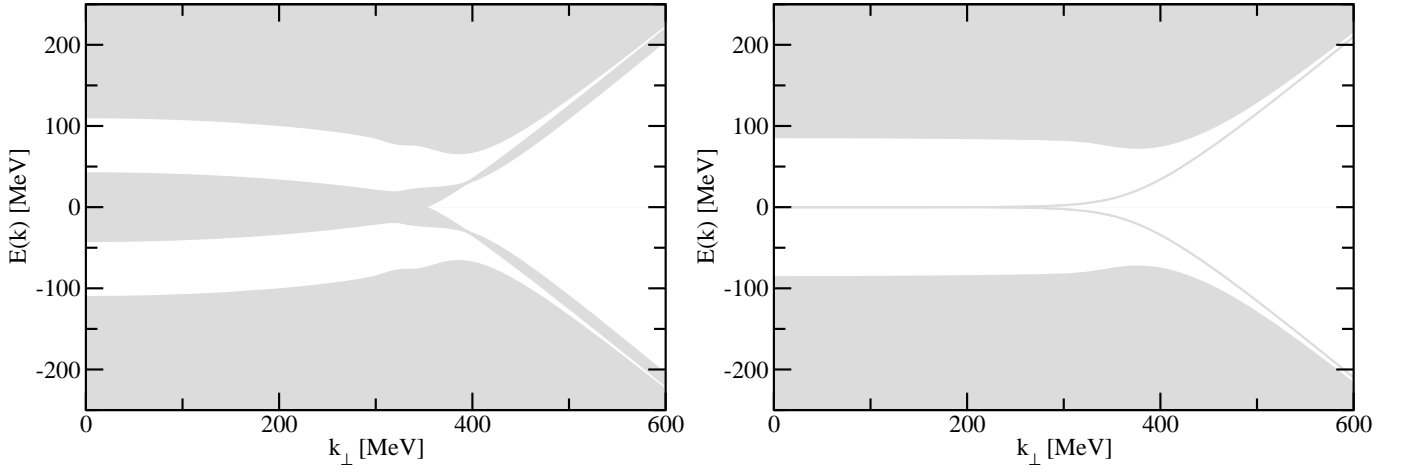


FIG. 9: Superposition of the eigenvalue spectra  $E_\lambda^{(0)}(\vec{k})$  of  $\mathcal{H}_{\Delta, \delta\mu=0}$  in the *B.Z.* along the momentum  $k_z$  parallel to  $\vec{q}$  as functions of the perpendicular momentum  $k_\perp$  (shaded areas). The spectra have been obtained for the gap functions of the energetically preferred ground state at  $\delta\mu = 0.7\Delta_{BCS}$  for fixed periods  $|\vec{q}| = 0.9\Delta_{BCS}$  (left) and  $|\vec{q}| = 0.2\Delta_{BCS}$  (right).

lead to infinitesimal changes in the eigenvalue spectra. Therefore, if  $\delta\mu$  lies in a gapped region, this variation will not change the numbers  $N_s(\vec{k})$ , which are, by definition, integer numbers. Consequently,  $\frac{\delta\Omega_0^{(2)}}{\delta\Delta_{\vec{q},k}} = 0$ , and the gap function is  $\delta\mu$  independent.<sup>6</sup>

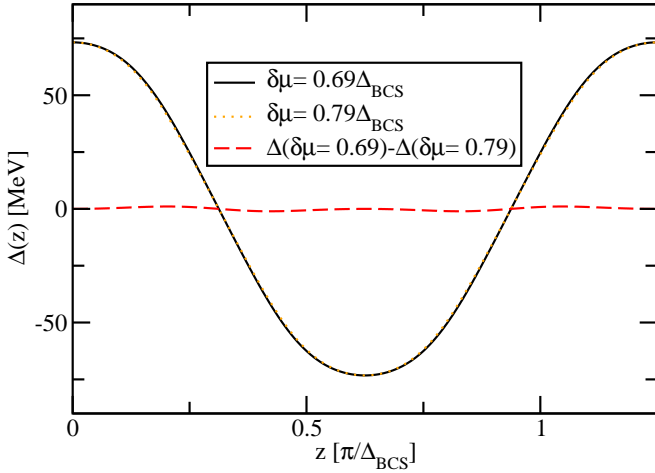


FIG. 10: Gap functions at  $\delta\mu = 0.69\Delta_{BCS}$  and  $\delta\mu = 0.79\Delta_{BCS}$ , and their difference for  $|\vec{q}| = 0.8\Delta_{BCS}$ .

In our case the excitation spectrum is not completely gapped. Nevertheless, when varying  $\delta\mu$  in the vicinity of  $0.7\Delta_{BCS}$ , the only eigenvalues interfering are those associated to the solitons and with momenta  $|\vec{k}| > \bar{\mu}$ . There

number is however relatively small and they are outside the Fermi ball. We can therefore expect their influence on the value of the thermodynamic potential and, hence, on the shape of the gap function to be very small.

To illustrate this property we present the gap function at  $\delta\mu = 0.69\Delta_{BCS}$  and  $\delta\mu = 0.79\Delta_{BCS}$  for  $|\vec{q}| = 0.8\Delta_{BCS}$  in Fig. 10. The gap functions, though taken at the lower and upper end of the LOFF window, appear almost identical. We conclude that the shape of the gap functions in the LOFF window for given  $|\vec{q}|$  is almost independent of  $\delta\mu$ .

We also note that the spatially averaged density difference between up and down quarks is given by

$$\langle\delta n\rangle = \langle n_u\rangle - \langle n_d\rangle = -\frac{\partial\Omega}{\partial\delta\mu}. \quad (78)$$

We thus get from the above equations

$$\langle\delta n\rangle = 4\left(n_s + \delta\mu\frac{\partial n_s}{\partial\delta\mu}\right), \quad (79)$$

where we have used that the implicit  $\delta\mu$  dependence through the gap functions drop out because of the gap equations. Moreover, as we have seen before,  $n_s$  is almost independent of  $\delta\mu$ , if  $\delta\mu$  is varied within the nearly gapped region. Therefore the second term on the right hand side is small and we find that the density difference is approximately proportional to the density of solitonic states,

$$\langle\delta n\rangle \approx 4n_s. \quad (80)$$

In particular, this implies that, unlike in the BCS phase, the density difference does not vanish if low-lying solitons are present. On the other hand,  $\langle\delta n\rangle$  is almost  $\delta\mu$  independent when  $\delta\mu$  is varied in the gapped regime.

<sup>6</sup> In our model, this property is slightly spoiled by the regularization, as already discussed for the BCS gap.

This gives rise to the very intuitive picture that the excess quarks are sitting in the solitons, whereas in the BCS-like plateaus of the gap functions the densities of up and down quarks are nearly equal. Here we should keep in mind that the period of the gap function and, hence, the soliton density, was kept constant in the above discussion. This explains why we found  $\langle \delta n \rangle$  to be  $\delta\mu$  independent. If we do not fix the period, but minimize the thermodynamic potential with respect to  $|\vec{q}|$ , as in Fig. 5,  $\Omega$  is no longer linear in  $\delta\mu$ , and  $\langle \delta n \rangle$  becomes  $\delta\mu$  dependent. In fact, we can turn this argument around and explain the  $\delta\mu$  dependence of  $|\vec{q}|$  by the preference of the system to accommodate more excess quarks with increasing  $\delta\mu$ .

### E. Comparison with analytical results in one spatial dimension

It is quite instructive to compare our results for the gap functions in three spatial dimensions with the analytically known solutions of the mean-field problem in one spatial dimension.

In 1 + 1-dimensions the mean-field problem can be approached in different ways and its first solution goes back to Peierls [39]. In terms of inverse scattering theory, the selfconsistently determined gap function has to generate a reflectionless (for a single bound state) or finite-gap potential in the Hamiltonian [40, 41] leading to a single band in the excitation spectrum. This is very similar to the feature displayed in Fig. 8 and Fig. 9 for small perpendicular momenta  $k_{\perp}$ . Related results have also been obtained in the Gross-Neveu model [43] and, recently, selfconsistent solutions have also been found for complex gap functions [44].

The case of a superconductor with two non-degenerate fermion species in 1 + 1-dimensions has been discussed in Ref. [45]. It was found that there is a transition at  $\delta\mu = \frac{2}{\pi}\Delta_{BCS}$  from the BCS phase to the solitonic phase, which persists to any larger value of  $\delta\mu$  at zero temperature. A selfconsistent solution of the gap function in this case is given by

$$\Delta_{1+1}(x) = \kappa\sqrt{\nu} \operatorname{sn}(\kappa(x - x_0); \nu), \quad (81)$$

where  $\operatorname{sn}(\xi; \nu)$  is a Jacobi elliptic function with elliptic modulus  $\nu^2$ . The Jacobi elliptic function has the properties  $\operatorname{sn}(0; \nu) = 0$ ,  $\frac{\partial}{\partial \xi} \operatorname{sn}(\xi; \nu)|_{\xi=0} = 1$ , and for  $0 \leq \nu < 1$  it is periodic in  $\xi$  with period  $4K(\nu)$ , where  $K(\nu)$  is the complete elliptic integral of the first kind. For the limiting cases, we have  $\operatorname{sn}(\xi; 0) = \sin \xi$  and  $\operatorname{sn}(\xi; 1) = \tanh \xi$ , i.e., for  $\nu \rightarrow 0$  the gap function becomes sinusoidal, whereas in the limit  $\nu \rightarrow 1$  we recover a single soliton.

With Eq. (81), the ground state is obtained by minimizing the thermodynamic potential in  $\kappa$  and  $\nu$ . It is remarkable that – apart from  $x_0$ , which is just an arbitrary shift – the gap functions can be characterized by only two parameters,  $\kappa$  and  $\nu$ , which can be related to the period  $4K(\nu)/\kappa$  and to the slope  $\kappa^2\sqrt{\nu}$  at the zero

crossings. In particular, the amplitude  $\kappa\sqrt{\nu}$  is completely determined by these two quantities. Also note that  $\kappa$  is just the slope at the zero crossings divided by the amplitude and we can therefore identify  $2/\kappa$  with the soliton size. Moreover, for constant  $\kappa$ , if  $\nu$  is varied within an interval close to 1, the period changes strongly, whereas the amplitude and the slope stay nearly constant. This is very similar to our observation in Fig. 2 that the amplitude and the shape of the transition region is almost independent of the period.

One may thus wonder, whether the one-dimensional gap functions in the 3 + 1 dimensional system are given by similar functions. Since, at least in the weakly coupled regime, all dynamics is constrained to a close shell around the Fermi surface, we could study the system on small patches at the Fermi surface, where the 3 + 1-dimensional problem can be reduced to 1 + 1-dimensional ones by applying a quasi-classical approximation [49]. The essential difference to the real 1 + 1 dimensional case is the fact that in 3 + 1 dimensions the momenta of the paired quarks are in general not parallel to the wave vector  $\vec{q}$  of the condensate. Therefore the quasi 1 + 1-dimensional problem needs to be solved for all directions [50, 51]. However, projecting the wave-vector of the condensate on a given direction renders the relation between shape and period of the order parameter and its amplitude to depend on the direction. For this reason, the 1 + 1-dimensional approach for obtaining a selfconsistent solution cannot be extended trivially to 3 + 1-dimensions.

On the other hand, we already observed in the discussion of Fig. 2 that, just as in 1 + 1 dimensions, the gap functions seem to depend on two independent scales,  $|\vec{q}|$  and  $\Delta_{BCS}$ , and that the latter determines both, the amplitude and the soliton size. Taking into account the complications discussed in the previous paragraph, this could be understood if the pairing is dominated by regions of the Fermi surface with a fixed azimuthal angle with respect to  $\vec{q}$ . This idea is also inspired by Ginzburg-Landau investigations where the pairing mechanism of the fermions shows up more explicitly [34]. In particular for the FF phase at weak coupling, the pairing is concentrated around rings on the Fermi surface where the relative angle between  $\vec{k}$  and  $\vec{q}$  is given by  $\cos \theta_{FF} \approx \frac{\delta\mu}{|\vec{q}|}$ . With this picture in mind we could imagine a similar regime of the Fermi ball to dominate the pairing in the general inhomogeneous phase with the order parameter varying in only one dimension. We would then expect that the amplitude of the gap function is again proportional to the inverse size of the soliton, but with a different proportionality constant than in the 1 + 1-dimensional case. Based on these arguments we suggest the fit

$$\Delta_{\text{fit}}(z) = A \operatorname{sn}(\kappa(z - z_0); \nu) \quad (82)$$

as a parameterization of our numerical results. To describe a gap function with period  $\frac{\pi}{|\vec{q}|}$  and to comply with our convention of taking  $\Delta(z)$  even with a maximum at



$z = 0$ , we choose

$$A = \Delta(0), \quad \kappa = \frac{4K(\nu)|\bar{q}|}{\pi}, \quad z_0 = -\frac{\pi}{4|\bar{q}|}. \quad (83)$$

Then the only fit parameter left is  $\nu$ . As a measure for the quality of the fit we consider the relative deviation

$$\frac{\|\Delta - \Delta_{\text{fit}}\|_2}{\|\Delta_{\text{fit}}\|_2} = \frac{\|\Delta - \Delta_{\text{fit}}\|_2}{\Delta(0)} \left( \frac{\nu K(\nu)}{K(\nu) - E(\nu)} \right)^{\frac{1}{2}}, \quad (84)$$

where  $E(\nu)$  is the complete elliptic integral of the second kind and  $\|\cdot\|_2$  is the  $L^2$ -norm.

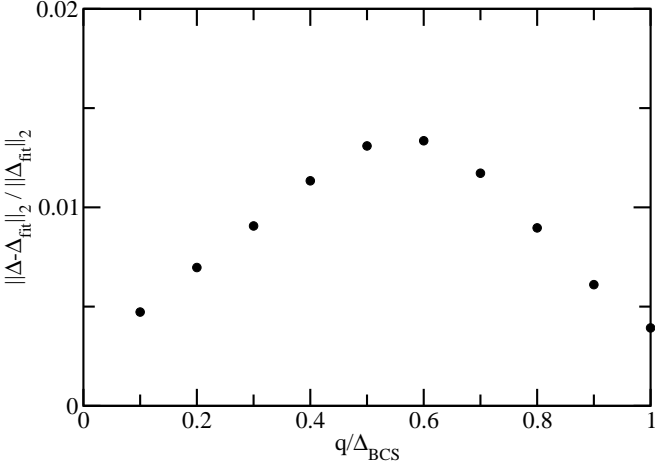


FIG. 11: Relative error between the numerically determined gap function and its best fit by Eq. (82) as function of the period. Here we have chosen  $\delta\mu = 0.7\Delta_{BCS}$ .

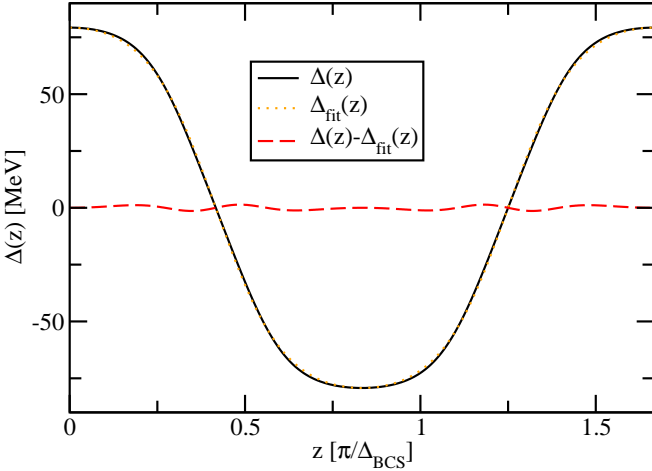


FIG. 12: Numerical result for gap function  $\Delta(z)$  compared to the best fit  $\Delta_{\text{fit}}(z)$  at  $\delta\mu = 0.7\Delta_{BCS}$  and  $|\bar{q}| = 0.6\Delta_{BCS}$ .

In Fig. 11 we present the relative error of our numerically obtained solutions compared to the best choice for  $\nu$

in the parameterization. We have chosen  $\delta\mu = 0.7\Delta_{BCS}$ . However, we remind that the gap function is very insensitive under variation of  $\delta\mu$ , as pointed out in the context of Fig. 10. It turns out that gap function is described remarkably well by the parameterization in Eq. (82) with only one fit parameter. The relative deviation in the  $L^2$ -norm is of the order of one percent<sup>7</sup>. To illustrate this further, we present the “worst” case at  $|\bar{q}| = 0.6\Delta_{BCS}$  in Fig. 12. The difference between the two functions is barely visible from plot.

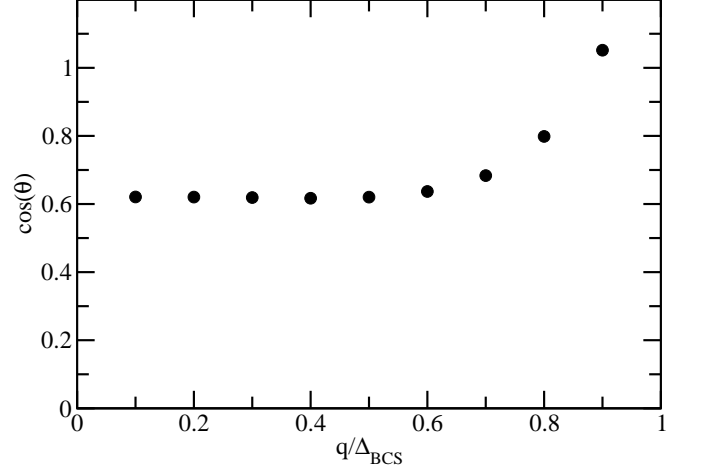


FIG. 13:  $\cos\theta$  as defined in Eq. (88) as function of  $|\bar{q}|$  for  $\delta\mu = 0.7\Delta_{BCS}$ .

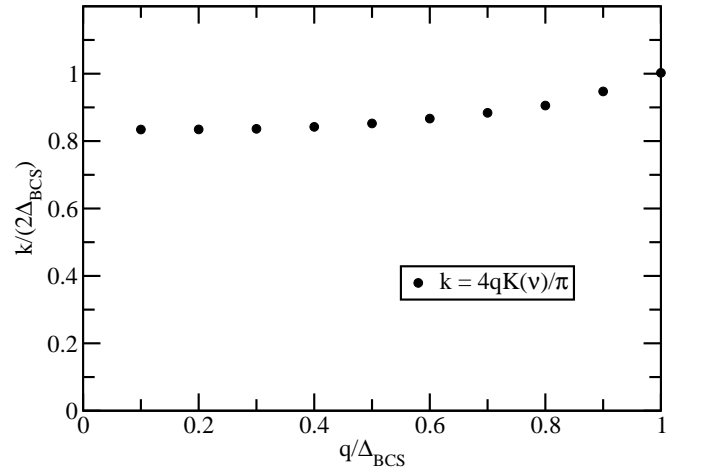


FIG. 14: Inverse soliton size  $\kappa$  as function of  $|\bar{q}|$  for optimum fit to numerical result.  $\delta\mu = 0.7\Delta_{BCS}$ .

Having found the astonishing agreement between the analytical form inspired from 1 + 1-dimensional investi-

<sup>7</sup> In view of the involved numerics and the marginal deviation we even do not want to exclude that the functions are identical.

gations and our numerical results, we are naturally lead to the assumption that the underlying dominant pairing mechanism is indeed dominated by fermions on the Fermi surface whose momenta have a fixed azimuthal angle measured from the direction of  $\vec{q}$ . If this is true, we would expect that the amplitude of the gap function is again proportional to  $\kappa$ , but with a different proportionality constant as in Eq. (81).

To establish this connection, which has so far been neglected in our parameterization, we assume that the pairing in directions  $\hat{n}$  with a particular azimuthal angle  $\theta$  to the direction of  $\vec{q}$  is dominant. Furthermore, we assume that the gap function in 3 + 1 dimensions is just given by the 1 + 1 dimensional result, Eq. (81), if we go along a line in such a direction, i.e.,

$$\Delta_{3+1}(z) = \Delta_{1+1}(x_\theta(z)), \quad (85)$$

where  $x_\theta(z) = \frac{z}{\cos\theta}$  is the coordinate in  $\hat{n}$  direction for a given  $z$  and

$$\Delta_{1+1}(x_\theta) = \kappa_\theta \sqrt{\nu} \operatorname{sn}(\kappa_\theta(x_\theta - x_{\theta,0}); \nu) \quad (86)$$

corresponds to Eq. (81). Hence, if we take  $\kappa_\theta = \kappa \cos\theta$ , we obtain

$$\Delta_{3+1}(z) = \kappa \cos\theta \sqrt{\nu} \operatorname{sn}(\kappa(z - z_0); \nu). \quad (87)$$

Comparing this with our ansatz Eq. (82) and Eq. (83) we get

$$\cos\theta = \frac{A}{\kappa\sqrt{\nu}} = \frac{\pi\Delta(0)}{4\sqrt{\nu}K(\nu)|\vec{q}|}. \quad (88)$$

This quantity is shown in Fig. 13. It turns out that our suggested picture breaks down at  $|\vec{q}| \gtrsim 0.9\Delta_{BCS}$ , where  $\cos\theta$  becomes larger than unity. This is related to the fact that the maximum of the gap function in our numerical results remains large also when its shape becomes more and more sinusoidal towards larger values for  $|\vec{q}|$ . In the limiting case we have  $\nu \rightarrow 0$  and Eq. (88) blows up.

On the other hand, we find that  $\cos\theta$  is almost constant for  $|\vec{q}| \lesssim 0.6\Delta_{BCS}$  at a value of  $\cos\theta \approx 0.62$ . This value corresponds to an opening angle  $2\theta \approx 100^\circ$ , somewhat larger than the typical opening angle of  $67^\circ$  in the FF phase. Note, however, that the situation in the FF phase is rather different. There the pairing can be understood most intuitively by shifting two Fermi spheres with radii  $\bar{\mu} + \delta\mu$  and  $\bar{\mu} - \delta\mu$  by  $\vec{q}$  in opposite directions [32]. In weak coupling, the physically relevant regime is then constrained around the intersection of the two Fermi surfaces, and one finds that  $\cos\theta_{FF} \approx \frac{\delta\mu}{|\vec{q}|}$ , as mentioned before. This means that  $\theta_{FF}$  is not constant as a function of  $|\vec{q}|$  and only possible if  $|\vec{q}| \gtrsim \delta\mu$ . However, since in the FF phase  $|\vec{q}|$  by itself is almost constant  $\sim 0.9\Delta_{BCS}$ , one typically finds  $\cos\theta_{FF} \approx 0.83$ .

For the general one-dimensional inhomogeneous phase, this is quite different. In this case, as we have seen,  $|\vec{q}|$  varies strongly and can become arbitrarily small. Nevertheless, according to Fig. 13, the associated angle is approximately constant, at least for  $|\vec{q}| \lesssim 0.6\Delta_{BCS}$ . This

regime, where FF pairing would not be possible at all, agrees roughly with the realm of the soliton lattice, see Fig. 2. Here the gap functions are no longer dominated by the lowest Fourier components  $\Delta_{\vec{q},\pm 1}$ , see Eq. (72), but higher harmonics are important as well. In fact, as we have seen earlier, the scale  $|\vec{q}|$  which is related to the inverse distance of the solitons becomes rather irrelevant for the dynamics, which is more closely related to the inverse soliton size  $\kappa$ .

The latter is displayed in Fig. 14. It is interesting to see that its value is comparable with the corresponding scale in the FF and indeed almost independent of the periodicity of the solitons. From the numbers which can be read off from the figure we find that the soliton size  $\frac{2}{\kappa}$  is about 0.3 - 0.4 in units of  $\frac{\pi}{\Delta_{BCS}}$ . This is in good agreement with Fig. 2.

#### IV. SUMMARY AND CONCLUSIONS

We have studied inhomogeneous pairing in relativistic imbalanced Fermi systems within a model of the Nambu–Jona-Lasinio type. The analysis was performed within mean-field approximation, but without restriction to the Ginzburg-Landau approach. In the set-up of the model we mainly focused on color superconducting phases, but the method is rather general and could be applied, e.g., to condensed matter physics or cold atomic gases as well.

In Sec. II we developed the general formalism for calculating the thermodynamic potential. We considered a certain class of gap functions, which are time independent and periodic in space. The color and flavor structure of the gap functions was chosen according to the most important pairing patterns in dense QCD, CFL and 2SC, but the extension to other phases is straight forward.

We pointed out that the regularization of the theory needs to be addressed with special care in order to get a consistent description of homogeneous and inhomogeneous phases. For instance, a straight-forward generalization of the three-momentum cutoff scheme to inhomogeneous systems leads to undesired artifacts. To avoid these problems we suggest a Pauli-Villars-like regularization scheme, which can be derived via proper-time regularization. In this scheme the divergencies are regulated by restricting the free energies of the quasiparticles, rather than their momenta. As a consequence, the results are rather insensitive to the choice of the cutoff parameter if the gap in the homogeneous phase is fixed. In particular, model independent results in the weak-coupling limit are reproduced correctly.

In Sec. III we discuss first numerical results obtained within this framework. To this end, we considered a simplified model with two fermion species at a chemical potential difference  $\delta\mu$ . Basically, this corresponds to a restriction to the 2SC phase in high-density approximation. Moreover, in order to keep the numerical effort at a tractable level, we restricted ourselves to real gap functions with general periodic structures in one dimension.

With this ansatz we found that the inhomogeneous solutions are favored against homogeneous superconducting (BCS) and normal conducting phases in a  $\delta\mu$ -window which is about twice as wide as for a simple plane-wave ansatz (FF phase). The main effect is seen at the lower end of this window, i.e., towards the boundary to the BCS phase. In this region we observe the formation of a soliton lattice. With lowering  $\delta\mu$  the distance between the solitons increases and eventually diverges at the critical point. In this way the inhomogeneous phase is continuously connected to the BCS phase. On the other hand, at the upper end of the window where the inhomogeneous phase is favored, the gap functions are sinusoidal, and the transition to the normal conducting phase is of first order.

It is worth noting that similar investigations of inhomogeneous phases of cold atoms in the unitary regime using a local density functional approach [52, 53] give exactly the opposite ordering of the phase transitions, i.e., first order for the transition from the homogeneous to the inhomogeneous phase and second order from the inhomogeneous to the normal phase. In our approach the behavior is however not unexpected: On the one hand side, mean-field investigations in  $1+1$ -dimensions find the same behavior [45] for the transition from the homogeneous to the inhomogeneous phase. On the other hand, the phase transition near the tricritical point at finite temperature can be analyzed in a generalized Ginzburg-Landau approach [54, 55]. The obtained results are perfectly consistent with ours. At this point we would also like to mention that within the generalized Ginzburg-Landau approach the energetically preferred inhomogeneous phase near the tricritical point has an order parameter only varying in one dimension, as in our investigation. It is however not clear whether this persists to zero temperature.

We also studied the quasiparticle excitations in the inhomogeneous ground state as functions of the momentum  $\vec{k}$  in the  $B.Z.$  As the inhomogeneous gap functions break the rotational symmetry, the spectra depend on both, the modulus and the direction of  $\vec{k}$ , leading to an interesting band structure. We found that the spectrum is “almost gapped” with a few low-lying modes which correspond to the solitons. As a consequence, the gap functions are almost insensitive to variations of  $\delta\mu$  if the period is kept constant.

Finally, we compared our solutions for the one-dimensional gap functions with the known analytical solutions of the corresponding  $1+1$  dimensional theory, i.e., Jacobi elliptic functions. We found that we can achieve an excellent fit in  $3+1$  dimensions, if we allow for one additional parameter. This can be interpreted as an effective  $1+1$  dimensional behavior which comes about if the pairing is dominated by fermions on the Fermi surface with momenta at a fixed azimuthal angle relative to  $\vec{q}$ .

The present paper is only a first step towards a more complete description of inhomogeneous pairing in rela-

tivistic systems. In the future, these studies should be extended in several directions:

We have calculated the gap functions as functions of a given chemical potential difference  $\delta\mu$ . It would be interesting to see how this translates into density profiles of the different fermion species. As argued at the end of section III D, we expect that the density difference will be close to zero at the constant plateaus of the gap functions and that it will be peaked at the zero crossings, i.e., in the solitons. Having worked this out, one could apply this to describe more physical situations, like globally neutral two-flavor quark matter in beta equilibrium or imbalanced atomic systems with fixed concentrations.

The analysis could be extended to finite temperature. In the context of color superconductivity one should also study other pairing patterns, like the CFL phase. Eventually, all this should be combined to obtain a phase diagram where homogeneous and inhomogeneous phases are treated on an equal footing. It would be interesting to see whether this can cure the problem of chromomagnetic instabilities in the phase diagram of neutral quark matter.

Of course, it would be desirable to relax the restriction to one-dimensional gap functions and to study two and three-dimensional crystalline structures. In fact, earlier investigations of crystalline color superconductivity revealed that three-dimensional crystals are the most favored inhomogeneous solutions [34, 35, 37]. These analyses, however, were performed in Ginzburg-Landau approximation, which turned out to be particularly problematic in the two-flavor case [34]. Moreover, the crystal structures were restricted to superpositions of a finite number of plane waves whose wave vectors all have the same length. This means that, e.g., the non-sinusoidal one-dimensional solutions which we found close to the BCS regime were not included. It is therefore not clear a priori which solutions are favored in a more complete analysis with arbitrary one-, two-, and three-dimensional periodic structures, in particular also because a one-dimensional solution is expected near the tricritical point [54, 55]. In principle, this could be studied within our framework. In practice, of course, the numerical solutions will become very involved, and one has to see how far one can get.

## Acknowledgments

We thank G. Basar, G. Dunne, M. Forbes, H. Gies, M. Mannarelli and especially K. Rajagopal for discussions and comments. This work was supported in part by funds provided by the German Research Foundation (DFG) under grant number Ni 1191/1-1, by the Helmholtz-University Young Investigator Grant No VH-NG-332 and by the U.S. Department of Energy (D.O.E.) under cooperative research agreement DE-FG0205ER41360.

**APPENDIX A: GINZBURG-LANDAU  
EXPANSION AND REQUIREMENTS ON  
REGULARIZATION PROCEDURE**

Starting from the mean-field thermodynamic potential, Eq. (20), we can derive a Ginzburg-Landau functional by expanding the potential in powers of the pairing gap. To that end, we split the inverse propagator, Eq. (19), into a free part and a gap dependent part,

$$S^{-1} = S_0^{-1} + \tilde{\Delta}, \quad (\text{A1})$$

where  $S_0 = S|_{\Delta=0}$  and expand the logarithm in Eq. (21) in a power series in  $\tilde{\Delta}$ :

$$\begin{aligned} & \text{Tr} \ln \left( \frac{1}{T} (S_0^{-1} + \tilde{\Delta}) \right) \\ &= \text{Tr} \ln \left( \frac{1}{T} S_0^{-1} \right) - \text{Tr} \sum_{n=1}^{\infty} \frac{1}{n} (-S_0 \tilde{\Delta})^n. \end{aligned} \quad (\text{A2})$$

Since  $S_0 \tilde{\Delta}$  has only off-diagonal terms in Nambu-Gor'kov space, only even  $n$  contribute to the trace. To lowest non-trivial order, we thus get

$$\begin{aligned} \Omega_{MF} &= \Omega_{MF}|_{\Delta=0} \\ &+ \frac{T}{4V} \text{Tr} (S_0 \tilde{\Delta} S_0 \tilde{\Delta}) + \frac{1}{4H} \sum_A \sum_{q_k} |\Delta_{A,q_k}|^2 \\ &+ O(\Delta^4). \end{aligned} \quad (\text{A3})$$

For the evaluation of the trace, we need the explicit expressions for  $S_0$  and  $\tilde{\Delta}$ . From Eq. (19) we get

$$S_0 = \begin{pmatrix} S_0^+ & 0 \\ 0 & S_0^- \end{pmatrix} \quad \text{and} \quad \tilde{\Delta} = \begin{pmatrix} 0 & \tilde{\Delta}^+ \\ \tilde{\Delta}^- & 0 \end{pmatrix}, \quad (\text{A4})$$

with

$$\begin{aligned} (S_0^\pm)_{p_m, p_n} &= (\not{p}_n \pm \not{p})^{-1} \delta_{p_m, p_n} \equiv S_0^\pm(p_n) \delta_{p_m, p_n}, \\ (\tilde{\Delta}^\pm)_{p_m, p_n} &= \sum_{q_k} \hat{\Delta}_{q_k} \gamma_5 \delta_{q_k, p_m - p_n}, \end{aligned} \quad (\text{A5})$$

and  $\tilde{\Delta}^- = -(\tilde{\Delta}^+)^\dagger$ . Furthermore, we get from Eq. (9)

$$\hat{\Delta}_{q_k} = \sum_A \Delta_{A,q_k} \tau_A \lambda_A, \quad (\text{A6})$$

while  $S_0$  is diagonal in flavor and color,

$$S_0^\pm = \text{diag}_{f_c} ((S_0^\pm)_{f_c}), \quad (\text{A7})$$

with flavor indices  $f \in \{u, d, s\}$  and color indices  $c \in \{r, g, b\}$ . Inserting these expressions into Eq. (A3), the trace is readily evaluated. As a consequence of momentum conservation, we find that unequal Fourier components of the gap function do not interfere at this order. Likewise, there is no interference between two components with different color-flavor indices. We thus obtain

an incoherent sum over  $|\Delta_{A,q_k}|^2$ , which can be combined with the sum in Eq. (A3) to get

$$\begin{aligned} \Omega_{MF} &= \Omega_{MF}|_{\Delta=0} \\ &+ \frac{1}{2} \sum_A \sum_{q_k} \tilde{\alpha}_{A,q_k} |\Delta_{A,q_k}|^2 + O(\Delta^4). \end{aligned} \quad (\text{A8})$$

The coefficients  $\tilde{\alpha}_{A,q_k}$  are given by

$$\begin{aligned} \tilde{\alpha}_{2,q_k} &= \\ &- \frac{T}{2V} \sum_{p_n} \left( \text{tr}_D [(S_0^+)_{ur}(p_n + q_k) \gamma_5 (S_0^-)_{dg}(p_n) \gamma_5] \right. \\ &\quad + \text{tr}_D [(S_0^+)_{ug}(p_n + q_k) \gamma_5 (S_0^-)_{dr}(p_n) \gamma_5] \\ &\quad + \text{tr}_D [(S_0^+)_{dr}(p_n + q_k) \gamma_5 (S_0^-)_{ug}(p_n) \gamma_5] \\ &\quad \left. + \text{tr}_D [(S_0^+)_{dg}(p_n + q_k) \gamma_5 (S_0^-)_{ur}(p_n) \gamma_5] \right) \\ &+ \frac{1}{4H}, \end{aligned} \quad (\text{A9})$$

and analogously for  $\tilde{\alpha}_{5,q_k}$  and  $\tilde{\alpha}_{7,q_k}$ . In the 2SC phase only  $\Delta_{2,q_k}$  is nonvanishing, and we may drop the index  $A$ . The coefficients then essentially depend on the chemical potential difference  $\delta\mu$ , defined in Eq. (49).

The remaining traces in Dirac space, denoted by  $\text{tr}_D$ , are trivial. As before, the sum over  $p_n$  should be read as a Matsubara sum and a sum over the three-momentum  $\vec{p}_n$ , cf. Eq. (14). In the infinite volume limit, the latter should be replaced by an integral. Moreover, we have to introduce a regularization procedure to render this integral finite.

As pointed out above, the quadratic term of the Ginzburg-Landau functional is an incoherent superposition of the contributions from the different Fourier components. In particular, the coefficients  $\tilde{\alpha}_{q_k}$  are completely independent of each other and should therefore be equal to the coefficients in the Fulde-Ferrell phase at given  $\vec{q}$  and  $\delta\mu$ .

The determination of  $\tilde{\alpha}(\vec{q}, \delta\mu)$  in the Fulde-Ferrell case is a well-known exercise (see e.g. Refs. [31, 32]). In a weak-coupling expansion at high densities one finds

$$\tilde{\alpha}(\vec{q}) = \frac{\bar{\mu}^2}{\pi^2} (\alpha(|\vec{q}|, \delta\mu) + \delta\alpha_{reg}), \quad (\text{A10})$$

where

$$\alpha(q, \delta\mu) = -1 + \frac{\delta\mu}{2q} \ln \left( \frac{q + \delta\mu}{q - \delta\mu} \right) - \frac{1}{2} \ln \left( \frac{\Delta_{BCS}^2}{4|q - \delta\mu|^2} \right), \quad (\text{A11})$$

while  $\delta\alpha_{reg}$  depends explicitly on the regularization in the sense that the cutoff dependence of this term cannot be absorbed in an observable, like  $\Delta_{BCS}$ . As we pointed out in section II C, such terms should be avoided in order to keep the results free from regularization artifacts. In fact, in the regularization schemes usually employed for the Fulde-Ferrell phase [31, 32], the dependence on the regularization can completely be absorbed into a  $\Delta_{BCS}$  dependence, and  $\delta\alpha_{reg}$  vanishes.

However, it is not obvious whether this regularization can be generalized to arbitrary gap functions in the thermodynamic potential. Using a sharp cutoff  $\Lambda$  for in- and out-going momenta instead, we obtain

$$\delta\alpha_{reg}^{cutoff} = \frac{|\vec{q}|\Lambda^2}{4(\Lambda - \bar{\mu})\bar{\mu}^2}. \quad (\text{A12})$$

This excludes this most naive regularization scheme. For the proper-time regularization introduced in section II C, on the other hand, we find

$$\delta\alpha_{reg}^{proper\ time} = 0 \quad (\text{A13})$$

in weak coupling. We therefore suggest to use this scheme for a consistent regularization of inhomogeneous phases.

Finally, we would like to add two comments: First, instead of starting from Eq. (21), the Ginzburg-Landau functional could be derived equally well by expanding Eq. (25). At  $T = 0$  this means that the Ginzburg-Landau expansion corresponds to a perturbative expansion of the eigenvalues of the Hamiltonian, with the pairing gap treated as perturbation. However, since some of the eigenvalues of the ‘‘unperturbed’’ Hamiltonian vanish at the Fermi surfaces of the particles, whereas the pairing gap is large, the perturbative expansion does actually not converge for the most interesting eigenvalues near the Fermi surfaces. As an example consider a BCS-like dispersion relation,

$$\begin{aligned} E(p) &= \sqrt{(p - \mu)^2 + |\Delta|^2} \\ &= |p - \mu| + \frac{|\Delta|^2}{2|p - \mu|} + O(|\Delta|^4), \end{aligned} \quad (\text{A14})$$

which obviously does not converge near  $p = \mu$ . The Ginzburg-Landau expansion may therefore suffer a similar problem.

Second, the Ginzburg-Landau expansion may be useful to identify the divergencies in the thermodynamic potential. In  $3 + 1$  dimensions it can be used to show that all divergencies can be absorbed by adding the expressions  $c_2 \int |\Delta(x)|^2$  and  $c_4 \int |\Delta(x)|^4$  with appropriate coefficients  $c_2$  and  $c_4$  to the thermodynamic potential.

## APPENDIX B: SYMMETRY OF THE EIGENVALUE SPECTRUM UNDER $\delta\mu$

In this appendix we discuss properties of the eigenvalue spectrum of the Hamiltonian  $\mathcal{H}_{\Delta, \delta\mu}$  in Eq. (51). For the case of a real gap function  $\Delta(x)$  we would like to show, that in terms of the eigenvalue spectrum  $\{E_\lambda\}$  of  $\mathcal{H}_{\Delta, \delta\mu}$  the eigenvalue spectrum of  $\mathcal{H}_{\Delta, -\delta\mu}$  is given by  $\{-E_\lambda\}$ . As a consequence, all eigenvalues of the total Hamiltonian  $\mathcal{H}_{HDE}$ , Eq. (50), come in pairs  $\{E_\lambda, -E_\lambda\}$ .

Restricting to real condensates, we can write

$$\mathcal{H}_{\Delta, \delta\mu} = H_0\sigma_3 + \Delta\sigma_1 - \delta\mu\mathbf{1}, \quad (\text{B1})$$

where  $(H_0)_{\vec{p}_m, \vec{p}_n} \equiv (p_m - \bar{\mu})\delta_{\vec{p}_m, \vec{p}_n}$ ,  $\Delta_{\vec{p}_m, \vec{p}_n} \equiv \Delta_{p_m - p_n}$  and  $\{\sigma_i\}$  are the conventional Pauli matrices. Here we used that the Fourier components obey  $\Delta_{q_k} = \Delta_{-q_k}^*$  for a real gap function, see Eq. (11). From  $\{\sigma_a, \sigma_b\} = 2\delta_{ab}\mathbf{1}$  we then obtain with  $J = i\sigma_2$

$$\mathcal{H}_{\Delta, 0}J = -J\mathcal{H}_{\Delta, 0}. \quad (\text{B2})$$

Consequently an eigenvector  $v$  with eigenvalue  $E$  will always come along with an eigenvector  $Jv$  with eigenvalue  $-E$ , i.e., eigenvalues of  $\mathcal{H}_{\Delta, 0}$  come in pairs  $(E_\lambda, -E_\lambda)$ .

More specifically we can choose the eigensystem of  $J$  as a basis in which

$$\mathcal{H}_{\Delta, 0} = U \begin{pmatrix} 0 & -H_0 + i\Delta \\ -H_0 - i\Delta & 0 \end{pmatrix} U^\dagger, \quad (\text{B3})$$

with

$$U = \frac{1}{\sqrt{2}} \begin{pmatrix} -i & i \\ 1 & 1 \end{pmatrix}. \quad (\text{B4})$$

Therefore we have

$$\mathcal{H}_{\Delta, 0}^2 = U \begin{pmatrix} H_0^2 + V_+ & 0 \\ 0 & H_0^2 + V_- \end{pmatrix} U^\dagger, \quad (\text{B5})$$

with

$$V_\pm = \Delta^2 \pm i[H_0, \Delta]. \quad (\text{B6})$$

One can easily show that the spectra of the two operators  $H_0^2 + V_\pm$  are identical and given by  $\{E_\lambda^2\}$ . This fact is sometimes referred to as being isospectral. The operators  $V_\pm$  are furthermore very similar to potentials of fermions and bosons in supersymmetric quantum mechanics with superpotential  $\Delta$ .

Turning on again the chemical potential shift, we note that

$$\mathcal{H}_{\Delta, \delta\mu} = \mathcal{H}_{\Delta, 0} - \delta\mu\mathbf{1}, \quad (\text{B7})$$

i.e.,  $\delta\mu$  just leads to a shift of the eigenvalues of  $\mathcal{H}_{\Delta, 0}$ . Hence, for each pair  $(E_\lambda, -E_\lambda)$  of the eigenvalues of  $\mathcal{H}_{\Delta, 0}$ , there is a corresponding pair  $(E_\lambda \mp \delta\mu, -E_\lambda \mp \delta\mu)$  of eigenvalues of  $\mathcal{H}_{\Delta, \pm\delta\mu}$ . Therefore we get the claimed connection between the spectrum of  $\mathcal{H}_{\Delta, \delta\mu}$  and  $\mathcal{H}_{\Delta, -\delta\mu}$ .

Note that, in this proof, we made explicitly use of the fact that the matrix  $\Delta$  is hermitian, which, in turn, was a consequence of our assumption that the gap function  $\Delta(x)$  is real. This is the case for the inhomogeneous solutions discussed in Sec. III C and thereafter, as well as for the BCS phase. It is not true for the FF phase, where the gap function is complex. However, in this case we can explicitly see from Eq. (71) that the eigenvalues  $E_\pm(\vec{k})$  go over into  $-E_\mp(-\vec{k})$  when we replace  $\delta\mu$  by  $-\delta\mu$ . Therefore, since we integrate over  $\vec{k}$  in Eq. (70),  $\mathcal{H}_{\Delta, \delta\mu}$  and  $\mathcal{H}_{\Delta, -\delta\mu}$  contribute equally to the thermodynamic potential.

- 
- [1] P. Fulde and R. A. Ferrell, Phys. Rev. **135**, A550 (1964).
- [2] A. I. Larkin and Yu. N. Ovchinnikov, Zh. Eksp. Teor. Fiz. **47**, 1136 (1964); Sov. Phys. JETP **20** 762 (1965).
- [3] I. Bloch, J. Dalibard and W. Zwerger, Rev. Mod. Phys. **80**, 885 (2008) [arXiv:0704.3011 [cond-mat.other]].
- [4] K. Rajagopal and F. Wilczek, arXiv:hep-ph/0011333.
- [5] M. G. Alford, Ann. Rev. Nucl. Part. Sci. **51**, 131 (2001) [arXiv:hep-ph/0102047].
- [6] T. Schäfer, arXiv:hep-ph/0304281.
- [7] D. H. Rischke, Prog. Part. Nucl. Phys. **52**, 197 (2004) [arXiv:nucl-th/0305030].
- [8] M. Buballa, Phys. Rept. **407**, 205 (2005) [arXiv:hep-ph/0402234].
- [9] I. A. Shovkovy, Found. Phys. **35**, 1309 (2005) [arXiv:nucl-th/0410091].
- [10] M. G. Alford, A. Schmitt, K. Rajagopal and T. Schäfer, arXiv:0709.4635 [hep-ph].
- [11] M. G. Alford, J. Berges and K. Rajagopal, Nucl. Phys. **B558**, 219 (1999) [hep-ph/9903502].
- [12] P. F. Bedaque, Nucl. Phys. A **697**, 569 (2002) [arXiv:hep-ph/9910247].
- [13] M. Buballa and M. Oertel, Nucl. Phys. A **703**, 770 (2002) [arXiv:hep-ph/0109095].
- [14] M. Alford and K. Rajagopal, JHEP **06**, 031 (2002) [hep-ph/0204001].
- [15] A. W. Steiner, S. Reddy and M. Prakash, Phys. Rev. **D66**, 094007 (2002) [hep-ph/0205201].
- [16] D. Nickel, R. Alkofer and J. Wambach, Phys. Rev. **D74**, 114015 (2006) [hep-ph/0609198].
- [17] S. B. Ruster, I. A. Shovkovy and D. H. Rischke, Nucl. Phys. **A743**, 127 (2004) [hep-ph/0405170].
- [18] S. B. Ruster, V. Werth, M. Buballa, I. A. Shovkovy and D. H. Rischke, Phys. Rev. **D72**, 034004 (2005) [hep-ph/0503184].
- [19] D. Blaschke, S. Fredriksson, H. Grigorian, A. M. Öztaş and F. Sandin, Phys. Rev. D **72**, 065020 (2005) [arXiv:hep-ph/0503194].
- [20] H. Abuki and T. Kunihiro, Nucl. Phys. **A768**, 118 (2006) [hep-ph/0509172].
- [21] D. Nickel, R. Alkofer and J. Wambach, Phys. Rev. D **77**, 114010 (2008) [arXiv:0802.3187 [hep-ph]].
- [22] A. M. Clogston, Phys. Rev. Lett. **9**, 266 (1962); B. S. Chandrasekhar, App. Phys. Lett. **1**, 7 (1962).
- [23] G. Sarma, J. Phys. Chem. Solids **24** 1029 (1963).
- [24] I. Shovkovy and M. Huang, Phys. Lett. B **564**, 205 (2003) [arXiv:hep-ph/0302142]; M. Huang and I. Shovkovy, Nucl. Phys. A **729**, 835 (2003) [arXiv:hep-ph/0307273].
- [25] E. Gubankova, W. V. Liu and F. Wilczek, Phys. Rev. Lett. **91**, 032001 (2003) [arXiv:hep-ph/0304016]; W. V. Liu and F. Wilczek, Phys. Rev. Lett. **90**, 047002 (2003) [arXiv:cond-mat/0208052].
- [26] M. Alford, C. Kouvaris and K. Rajagopal, Phys. Rev. Lett. **92**, 222001 (2004) [arXiv:hep-ph/0311286]; Phys. Rev. D **71**, 054009 (2005) [arXiv:hep-ph/0406137].
- [27] M. Huang and I. A. Shovkovy, Phys. Rev. D **70**, 051501 (2004) [arXiv:hep-ph/0407049].
- [28] R. Casalbuoni, R. Gatto, M. Mannarelli, G. Nardulli and M. Ruggieri, Phys. Lett. B **605**, 362 (2005); Erratum-ibid. B **615**, 297 (2005) [arXiv:hep-ph/0410401].
- [29] F. Neumann, M. Buballa and M. Oertel, Nucl. Phys. A **714**, 481 (2003) [arXiv:hep-ph/0210078].
- [30] S. Reddy and G. Rupak, Phys. Rev. C **71**, 025201 (2005) [arXiv:nucl-th/0405054].
- [31] R. Casalbuoni and G. Nardulli, Rev. Mod. Phys. **76**, 263 (2004) [arXiv:hep-ph/0305069].
- [32] M. G. Alford, J. A. Bowers and K. Rajagopal, Phys. Rev. D **63**, 074016 (2001) [arXiv:hep-ph/0008208].
- [33] I. Giannakis and H. C. Ren, Phys. Lett. B **611**, 137 (2005) [arXiv:hep-ph/0412015]; I. Giannakis, D. f. Hou and H. C. Ren, Phys. Lett. B **631**, 16 (2005) [arXiv:hep-ph/0507306].
- [34] J. A. Bowers and K. Rajagopal, Phys. Rev. D **66**, 065002 (2002) [arXiv:hep-ph/0204079].
- [35] R. Casalbuoni, R. Gatto, N. Ippolito, G. Nardulli and M. Ruggieri, Phys. Lett. B **627**, 89 (2005); Erratum-ibid. B **634**, 565 (2006) [arXiv:hep-ph/0507247].
- [36] M. Mannarelli, K. Rajagopal and R. Sharma, Phys. Rev. D **73**, 114012 (2006) [arXiv:hep-ph/0603076].
- [37] K. Rajagopal and R. Sharma, Phys. Rev. D **74**, 094019 (2006) [arXiv:hep-ph/0605316].
- [38] P. G. de Gennes, *Superconductivity of Metals and Alloys* (Benjamin, New York, 1966).
- [39] R. Peierls, *The Quantum Theory of Solids* (Oxford, 1955).
- [40] R. F. Dashen, B. Hasslacher and A. Neveu, Phys. Rev. D **12**, 2443 (1975).
- [41] S. S. Shei, Phys. Rev. D **14**, 535 (1976).
- [42] B. Horowitz, Phys. Rev. Lett. **46**, 742 (1981).
- [43] V. Schön and M. Thies, arXiv:hep-th/0008175; M. Thies, J. Phys. A **39**, 12707 (2006) [arXiv:hep-th/0601049].
- [44] G. Basar and G. V. Dunne, Phys. Rev. Lett. **100**, 200404 (2008) [arXiv:0803.1501 [hep-th]]; G. Basar and G. V. Dunne, arXiv:0806.2659 [hep-th].
- [45] K. Machida and H. Nakanishi, Phys. Rev. B **30**, 122 (1984).
- [46] G. Eilenberger, Z. Phys. **214** 195 (1968).
- [47] A. I. Larkin and Yu. N. Ovchinnikov, Zh. Eksp. Teor. Fiz. **55**, 2262 (1968); Sov. Phys. JETP **28** 1200 (1969).
- [48] D. Waxman and G. Williams, J. Phys. A **25**, 1593 (1992).
- [49] A. F. Andreev, Sov. Phys. JETP **19**, 1228 (1964).
- [50] D. Waxman, Phys. Rev. Lett. **72**, 570 (1994).
- [51] I. Kosztin, S. Kos, M. Stone and A. J. Leggett, Phys. Rev. B **58**, 9365 (1998).
- [52] A. Bulgac and M. M. Forbes, [arXiv.org:0804.3364].
- [53] A. Bulgac and M. M. Forbes, [arXiv.org:0808.1436].
- [54] A. I. Buzdin and H. Kachkachi, Phys. Lett. A **225**, 1341 (1997) [arXiv:cond-mat/9611153].
- [55] M. Houzet, Y. Meurdesoif, O. Coste and A. I. Buzdin, Physica C **316**, 89 (1999).